were used as wild-type control mice. JMJD6 knock-out embryonic day 14.5 (E14.5) embryos were obtained by crossing heterozygous JMJD6 mutant mice.

Antibodies, Plasmids, and Cell Lines—The following antibodies were used: anti-JMJD6 rabbit polyclonal antibody (ab10526, Abcam), and anti-β-actin mouse monoclonal antibody (GTX26276, GeneTex). Human *JMJD6* cDNA was cloned into pGEX-6p-1 (GE Healthcare) and pcDNA5/FRT/TO (Invitrogen). Doxycycline (Dox)-inducible JMJD6 stable cells were generated using the Flp-In T-REx system (Invitrogen) according to the manufacturer's instructions. JMJD6 expression was induced by Dox (final concentration, 0.5 μg/ml; TaKaRa, Tokyo, Japan). J1 mouse ES cells were obtained from ATCC (Manassas, VA) and maintained in DMEM with 15% fetal bovine serum (FBS), nonessential amino acids, 2-mercaptoethanol, and leukemia inhibitory factor. Flp-In T-Rex 293 cells were obtained from Invitrogen and the Dox-inducible JMJD6 stable 293 cells were maintained in DMEM with 10% FBS, 10% tetracycline-free FBS, hygromycin B (100 μg/ml), and blasticidin S (15 μg/ml).

Quantitative RT-PCR—For qRT-PCR reactions, specific primers and probes for mouse JMJD6 (forward, 5′-GACCCGGCACAACTACTACG-3′; reverse, 5′-CTCTTGTGCATTGAGCAGAAC-3′) and mouse GAPDH (forward, 5′-CCATGTTTGTGATGGGTGTG-3′ and reverse, 5′-ACTGTGGTCATGAGCCCTTC-3′) were used. PCR reactions were performed using the TaKaRa Thermal Cycler Dice® Real Time System Single following the manufacturer's instructions. Amplification conditions were 30 s at 95 °C and then 40 cycles each consisting of 5 s at 95 °C and 30 s at 60 °C.

Purification of GST-JMJD6 and in Vitro Binding Assay—Recombinant GST-JMJD6 was expressed in BL21-CodonPlus DE3-RIL cells. The transformed bacteria were incubated in L-Broth media with 0.1 mM isopropyl 1-thio-β-D-galactopyranoside at 16 °C overnight. Following this, the bacteria were lysed in sonication buffer (150 mM NaCl, 20 mM Tris-HCl (pH 7.5), 2 mM EDTA, 10% glycerol, 1% Triton X, and 0.8 mg/ml lysozyme) by sonication. GST-JMJD6 was purified using glutathione-Sepharose 4FF (GE Healthcare) and eluted by glutathione. The purified proteins were incubated with biotin-labeled histone $H3_{1-21}$ peptides (12–405, Millipore, Billerica, MA) or recombinant full-length histone H4 (14–697, Millipore) in 0.1% Nonidet P-40 lysis buffer (150 mM NaCl, 0.1% Nonidet P-40, and 50 mM Tris-HCl (pH 8.0)) for 1 h at 4 °C. The biotin-labeled histone $H3_{1-21}$ peptides were pulled down with interacting proteins by streptavidin Sepharose (S951, Invitrogen). Full-length histone H4 was immunoprecipitated with anti-JMJD6 rabbit polyclonal antibody (ab10526, Abcam), which was also used for Western blotting.

In Vitro Hydroxylation Assay—To perform the enzyme assay, GST-JMJD6 was prepared as described above. Extracted GST-JMJD6 was concentrated using a 50 K column (Millipore), and its buffer was replaced with 50 mM Tris-HCl (pH 7.5) by dialysis using EasySep (TOMY, Tokyo, JAPAN). Purity of GST-JMJD6 was assessed by Coomassie Brilliant Blue staining. The enzyme assay was performed in 50 mM Tris-HCl (pH 7.5) buffer containing 500 μM α-ketoglutarate, 100 μM L-ascorbate, 100 μM $Fe(NH_4)_2SO_4$, 10 μM GST-JMJD6, and 20 μM histone peptides.

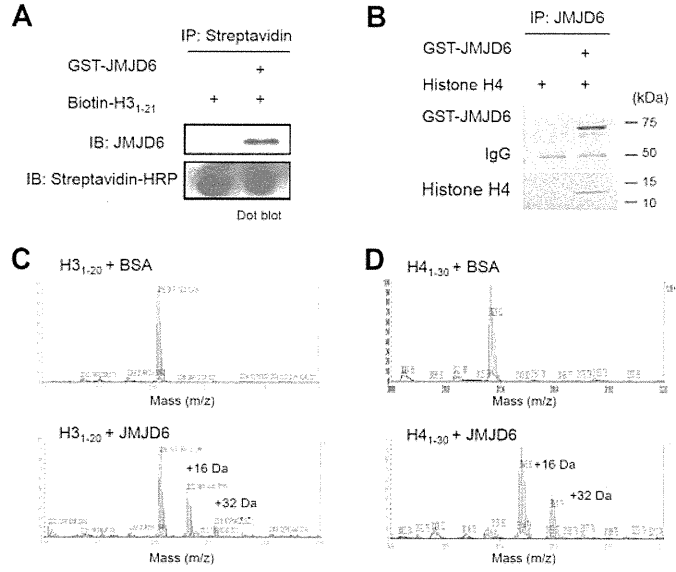

FIGURE 1. **JMJD6 interacts with and hydroxylates histone H3 and H4 *in vitro*.** *A* and *B*, *in vitro* pulldown assay. Biotin-labeled histone $H3_{1-21}$ peptides (*A*) or recombinant histone H4 (*B*) were incubated with or without GST-JMJD6, pulled down by streptavidin-Sepharose, and detected by dot blot using streptavidin-HRP (*A*) or Coomassie Brilliant Blue (*CBB*) staining (*B*). Pulled down GST-JMJD6 was detected by Western blotting using anti-JMJD6 antibody (*A*) or Coomassie Brilliant Blue staining (*B*). *C* and *D*, enzymatic activity of GST-JMJD6 was measured by MS analysis. Histone $H3_{1-20}$ (*C*) and $H4_{1-30}$ (*D*) peptides were served as substrates. BSA was used as a negative control. *IB*, immunoblot.

Protein purification and the enzyme assay were performed on the same day to avoid reduction of enzymatic activity of JMJD6.

MS Analysis—Peptides treated with JMJD6 were acidified with trifluoroacetic acid (TFA; final concentration, 0.5%) and absorbed with ZipTipC18. The captured peptides were washed with 0.1% TFA with 2% acetonitrile once and eluted with 0.5 μl of the matrix solution (4 mg/ml cyano-4-hydroxycinnamic acid, 0.1% TFA, 70% acetonitrile) onto the MALDI target plate (AB Sciex, Foster City, CA). The spotted samples were analyzed with the reflectron mode of 4800 plus MALDI-TOF-TOF mass spectrometer (AB Sciex).

Purification of Histones and Detection of 5-Hydroxylysine by Amino Acid Composition Analysis—Histones H2A/H2B and H3/H4 were separately purified from tissues or culturing cells using a histone purification kit (Active Motif, Carlsbad, CA) according to the manufacturer's instructions. The extracted histones were separated by SDS-PAGE, transferred to a membrane (Immobilon-P^{SQ}, Millipore), and stained by Coomassie Brilliant Blue. The transferred histones were used for amino acid composition analysis to detect 5-hydroxylysine.

The JMJD6-treated peptides or the purified histones were hydrolyzed in 6 N HCl vapor at 110 °C for 20 h. The acid hydrolysates of the peptides were derivatized with 6-aminoquinolyl-*N*-hydroxysuccinimidyl carbamate, and 6-aminoquinolylcarbamyl amino acid thus obtained was quantified by ion-pair chromatography using tetramethylammonium bromide on a C18-reversed phase column (L-column 2, 3.0 mm, inner diameter × 250 mm, 3 μm, CERI, Tokyo, Japan) (9). Each amino acid was separated by HPLC. The acid hydrolysates of the histones were purified on a graphitic carbon column (Hypercarb, 2.1 mm, inner diameter × 100 mm, 3 μm, Thermo Fisher Scien-

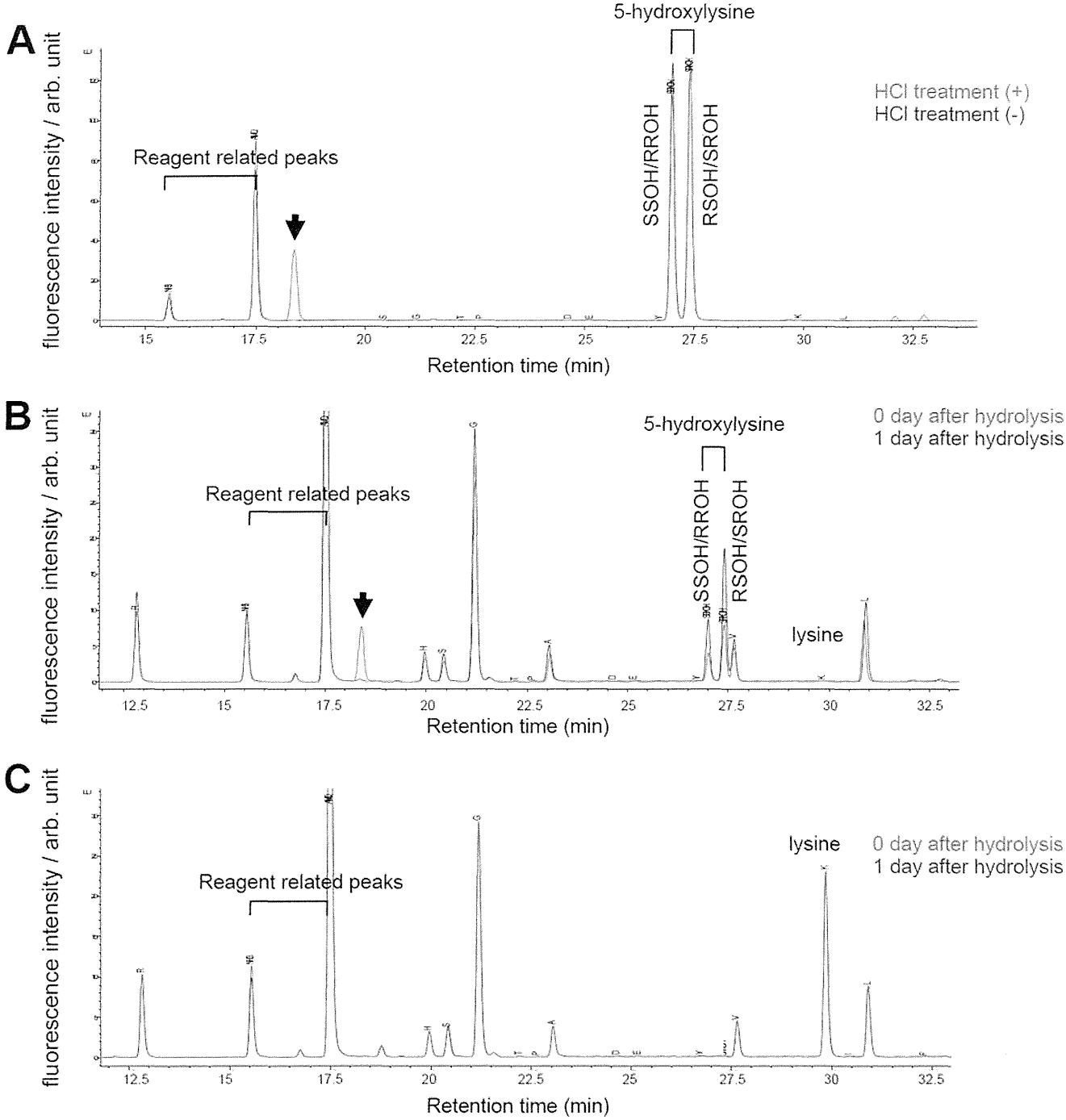

FIGURE 2. **Establishment of amino acid composition analysis for detecting 5-hydroxylysine.** *A*, analysis of simplicial synthetic SR-hydroxylysine and synthetic racemic mixture (*SS/RR/RS/SR*) of 5-hydroxylysine either treated with (*red*) or without (*blue*) HCl. *B* and *C*, analysis of $H4_{1-20}$ peptides including synthetic 5-hydroxylysine (*B*) and unmodified $H4_{1-20}$ peptides (*C*). The peptides were analyzed in the same day of hydrolysis (*red*) or next day of hydrolysis (*blue*). The *arrow* indicates a 5-hydroxylysine derived peak, which possibly corresponds to a lactone derivative, 3-amino-6-(aminomethyl)oxan-2-one. *SSOH/RROH*, 2*S*,5*S*-/2*R*,5*R*-hydroxylysine; *RSOH/SROH*, 2*R*,5*S*-/2*S*5*R*-hydroxylysine; *arb. unit*, arbitrary units.

tific, Inc., Waltham, USA), and a fraction including 5-hydroxylysine was derivatized with 6-aminoquinolylcarbamyl. The 6-aminoquinolylcarbamyl amino acids were separated on a C18-reversed phase column (Inertsustain C18HP, 3.0 mm, inner diameter × 250 mm, 3 μm, GL Sciences, Tokyo, Japan) and quantified. Synthetic racemic mixture of DL-5-hydroxylysine (catalog no. H0377, Sigma-Aldrich), and 2*S*,5*R*-hydroxylysine (catalog no. 55501, Sigma-Aldrich) were used as standards.

In Vitro Histone Acetyltransferase (HAT) Assay—The *in vitro* p300 colorimetric HAT assay was performed according to a protocol from BIOMOL (Plymouth Meeting, PA). In brief, the catalytic domain of human p300 (catalog no. SE-451, BIOMOL) and the indicated amount of control histone $H4_{1-23}$ peptides or 5-hydroxylysine containing histone $H4_{1-23}$ peptides, in which all lysines were substituted to 5-hydroxylysine (Sigma-Genosys, Hokkaido, Japan), were incubated in 50 μl of assay buffer (50 mM HEPES/NaOH (pH 7.9), 0.1 mM EDTA, 50 μg/ml BSA) in

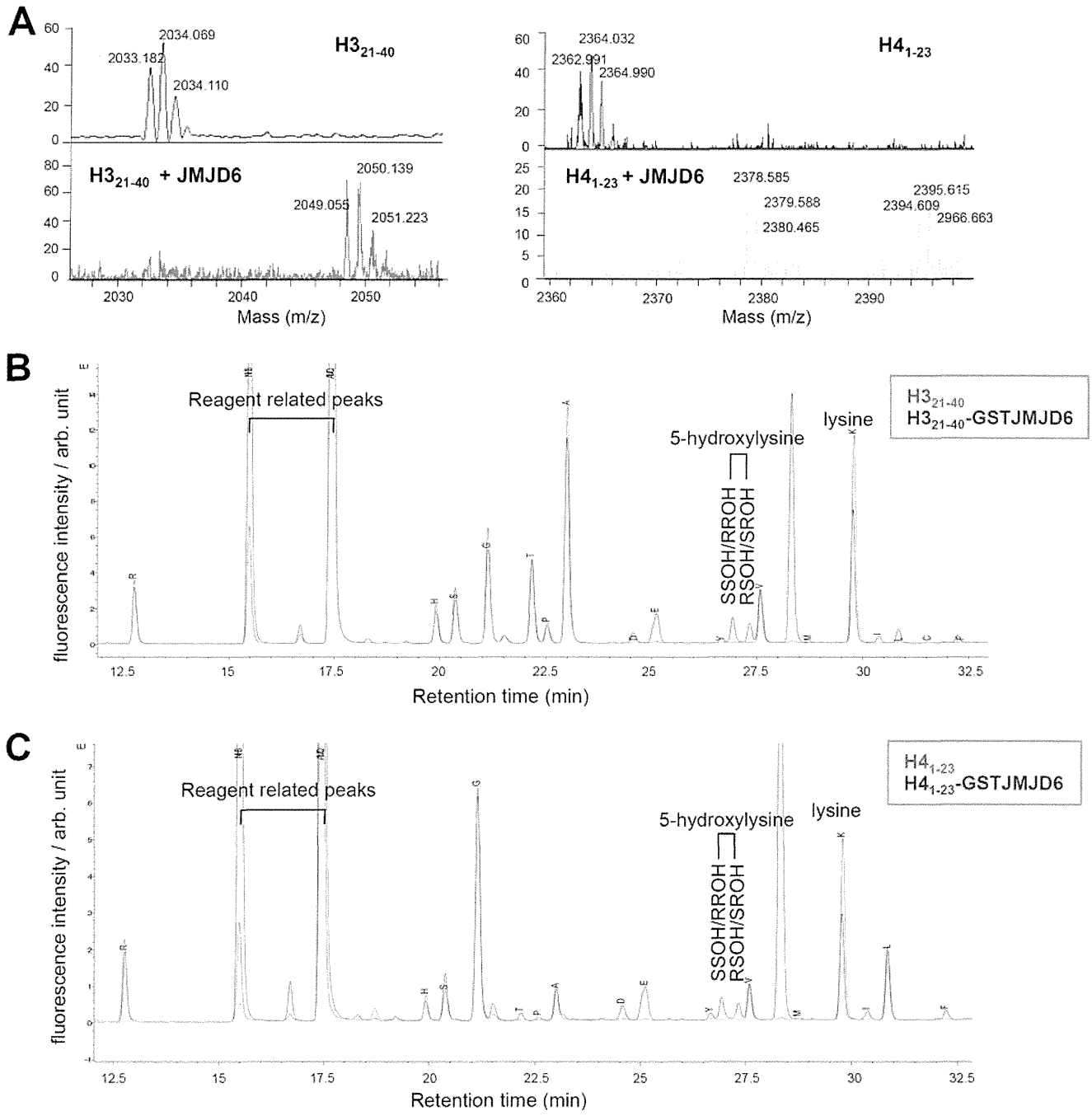

FIGURE 3. **JMJD6 hydroxylates histone H3 and H4 peptides detected by amino acid composition analysis.** *A*, hydroxylation of $H3_{21-40}$ and $H4_{1-23}$ peptides by GST-JMJD6 was confirmed by MS analysis. *B* and *C*, results of amino acid composition analysis of $H3_{21-40}$ (*B*) and $H4_{1-23}$ (*C*) peptides treated with (*blue*) or without (*red*) GST-JMJD6. *SSOH/RROH*, 2*S*,5*S*/2*R*,5*R*-hydroxylysine; *RSOH/SROH*, 2*R*,5*S*-/2*S*,5*R*-hydroxylysine; *arb. unit*, arbitrary units.

the presence of acetyl-coenzyme A (CoA, Sigma-Aldrich) at 37 °C. The reaction was stopped by adding 100 μl of quenching buffer (3.2 M guanidinium HCl, 100 mM Na_2HPO_4/NaH_2PO_4 (pH6.8)) at the indicated times. Following this, 50 μl of 2 mM 5,5′-dithiobis-2-nitrobenzoic acid (Sigma-Aldrich) in 100 mM Na_2HPO_4/NaH_2PO_4 (pH 6.8) was added, and absorbance at 405 nm was read by a spectrophotometer (ARVO MX/Light 1420 Multilabel/Luminescence Counter, PerkinElmer Life Sciences). The transfer of an acetyl group from an acetyl-CoA to the ϵ-amino group of lysine residues was quantified by measurement of the thiol group of CoA. A standard curve was generated using β2-mercaptoethanol.

In Vitro Histone Methyltransferase Assay—The *in vitro* histone methyltransferase assay was performed as described previously (10), except for slight modifications. In brief, a fixed amount of purified baculovirus-produced recombinant SMYD3 (1 μM) was incubated with indicated histone peptides, which were also used for the *in vitro* HAT assay, and 1 μCi of *S*-adenosyl-L-methionine (AdoMet; GE Healthcare) as the methyl donor in a mixture of 60 μl of methylase activity buffer (50 mM Tris-HCl (pH 8.5), 100 mM NaCl, 10 mM dithiothreitol) at 30 °C. The incorporated ^{3}H-labeled methyl groups in the substrates were measured by a scintillation counter after filter binding (units, cpm). The concentration

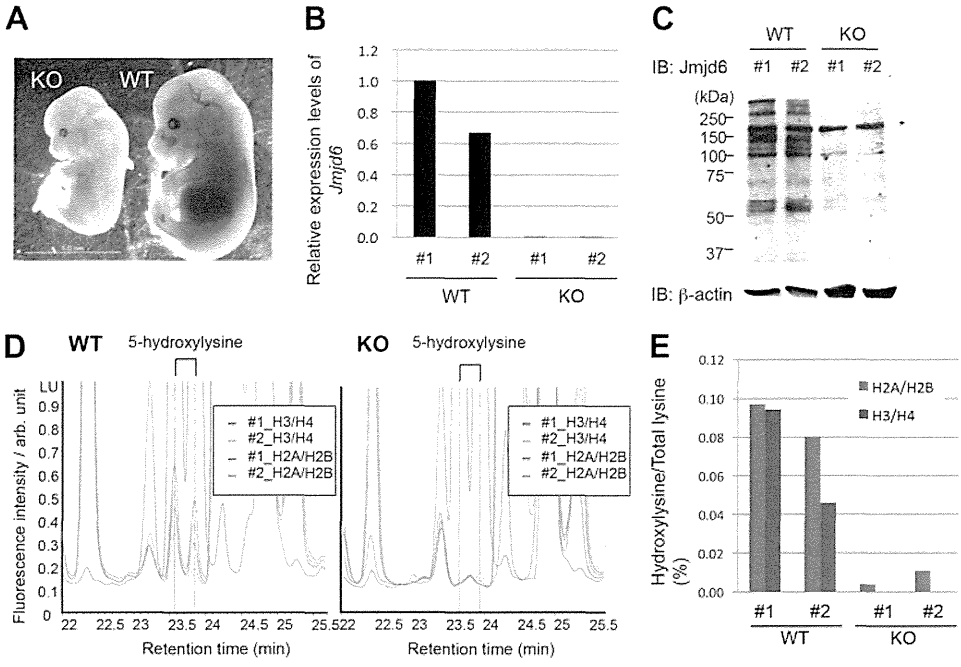

FIGURE 4. **JMJD6 hydroxylates histones H2A/H2B and H3/H4 in mouse embryos.** *A*, a representative image of JMJD6 knock-out and wild-type E14.5 embryos. *B*, *JMJD6* knock-out was confirmed by qRT-PCR. GAPDH was used as an internal control. *C*, JMJD6 knock-out was confirmed by Western blotting. The *asterisk* indicates a nonspecific band. β-Actin was used as a loading control. *D*, result of amino acid composition analysis of histones derived from two Jmjd6 wild-type (*left*) and knock-out (*right*) E14.5 embryos. *E*, % of 5-hydroxylysine in total lysine of histones H2A/H2B (*blue*) and H3/H4 (*red*) was calculated from the HPLC data (*D*). *IB*, immunoblot; *arb. unit*, arbitrary units.

(nM) of the methylated substrate was calculated based on the basis of radioactivity.

RESULTS

JMJD6 Effectively Hydroxylates Histone Lysyl Residues in Vitro—During screening of UHRF1-interacting proteins, we identified JMJD6 as a novel binding partner of UHRF1 (data not shown). Because UHRF1 recognizes hemimethylated DNA and histone modifications, we assumed that JMJD6 might be recruited by UHRF1 to nucleosomes and modify histone lysyl residues. *In vitro* experiments showed that recombinant GST-JMJD6 possessed the ability to bind to histone $H3_{1-20}$ tail and histone H4 (Fig. 1, *A* and *B*) and hydroxylate multiple lysyl residues in the N-terminal tails of histone $H3_{1-20}$ and $H4_{1-30}$, which was detected as of 16, 32, or 48 Da shifts by MS analysis (Fig. 1, *C* and *D*); subsequent MS/MS analysis revealed that JMJD6 mediates monohydroxylation of lysyl residues. As indicated by Webby *et al.* (1), JMJD6 preferentially hydroxylated lysyl residues in the basic peptides, and no apparent sequence preference was observed *in vitro* (data not shown).

Next, we established a sensitive hydroxylysine detection method based on amino acid composition analysis as an alternative to the MS-based method. For amino acid composition analysis, we briefly hydrolyzed peptides or proteins with HCl and separated each amino acid residue by reversed phase HPLC to detect 5-hydroxylysine. To evaluate this method, we first performed reversed phase HPLC using simplicial synthetic 2*S*,5*R*-hydroxylysine and synthetic racemic mixture of 5-hydroxylysine composed of 2*S*,5*S* (*SS*)-, 2*R*,5*R* (*RR*)-, 2*R*,5*S* (*RS*)-, and 2*S*,5*R* (*SR*)-stereoisomers (Fig. 2*A*). We detected two peaks corresponding to *SS*/*RR*- and *RS*/*SR*-hydroxylysine by analyzing these synthetic 5-hydroxylysines without HCl treatment (Fig. 2*A*). After HCl treatment of these synthetic 5-hydroxylysines, another peak was appeared (Fig. 2*A*, *arrow*). This peak possibly corresponds to a lactone derivative, 3-amino-6-(aminomethyl)oxan-2-one, generated by dehydration condensation between C5 hydroxyl group and carboxyl group, which is described in a previous report (11). Next, we evaluated the method using unmodified $H4_{1-23}$ peptides and 5-hydroxylysine containing $H4_{1-23}$ peptides in which all the lysines at positions 5, 8, 12, and 20 were substituted with 5-hydroxylysines. After hydrolysis of these peptides, we detected two peaks corresponding to *SS*/*RR*- and *RS*/*SR*-hydroxylysine only in the 5-hydroxylysine containing peptides but not in the unmodified peptides (Fig. 2, *B* and *C*). We also detected the peak of the possible lactone derivative in the 5-hydroxylysine containing peptides by reversed phase HPLC performed in the same day of hydrolysis, but the peak disappeared in the next day of hydrolysis, indicating that the derivative is unstable. Because quantification of the derivative is technically difficult, we only quantified *SS*/*RR*- and *RS*/*SR*-hydroxylysine.

Using this method, we analyzed $H3_{21-40}$ and $H4_{1-23}$ peptides treated with or without recombinant GST-JMJD6. First, we confirmed hydroxylation of the peptides by GST-JMJD6 by MS analysis (Fig. 3*A*). Then, the peptides were separated from the enzyme reaction mixture, by reversed phase HPLC. The separated peptides were treated with HCl, and each amino acid residue was separated by reversed phase HPLC (Fig. 3, *B* and *C*). Comparison of the chromatograph between amino acids derived from the JMJD6-treated and -untreated peptides identified two additional peaks in the peptides treated with JMJD6, which are matched with the standard synthetic 5-hydroxylysine (Fig. 3, *B* and *C*).

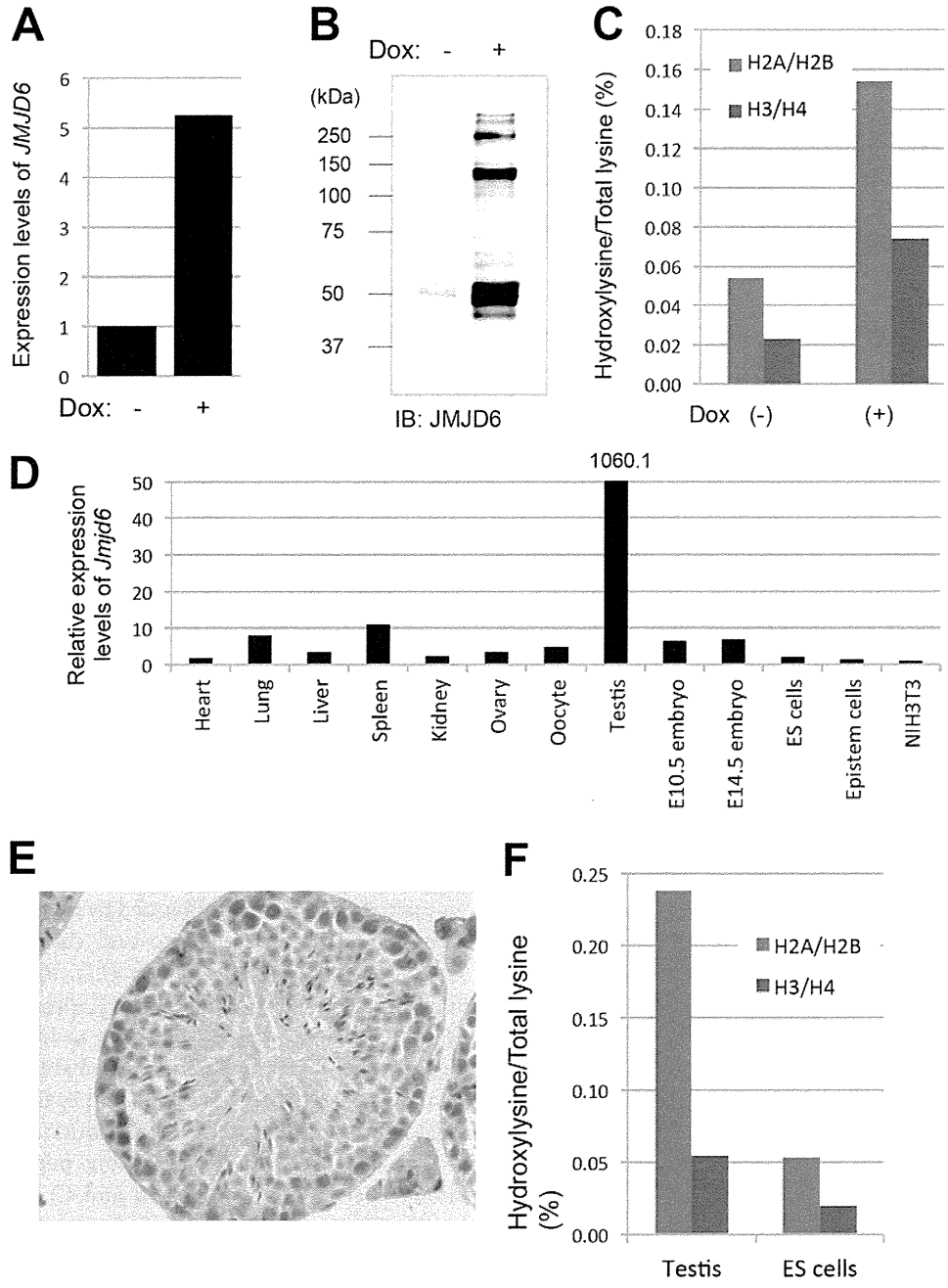

FIGURE 5. **Amount of 5-hydroxylysine in JMJD6 overexpressed HEK 293 cells, mouse testis, and ES cells.** *A*, expression levels of *JMJD6* in Dox-inducible JMJD6 stable cells were examined by qRT-PCR before and after 48-h Dox induction. *B*, induction of JMJD6 by Dox in the cells was confirmed by Western blotting. *C*, amino acid composition analysis of histones derived from Dox-inducible JMJD6 stable cell lines. The *blue* and *red bars* indicate % of 5-hydroxylysine in the total lysine of histone H2A/H2B and in the H3/H4, respectively. *D*, relative expression levels of *Jmjd6* in various mouse tissues and cells were examined by qRT-PCR. *E*, expression of Jmjd6 in a 6-month-old mouse testis was examined by immunohistochemistry. *F*, amino acid composition analysis of histones derived from 6-month-old mouse testis and J1 ES cells. The *blue* and *red bars* indicate % of 5-hydroxylysine in the total lysine of histone H2A/H2B and in the H3/H4, respectively.

JMJD6 Hydroxylates Histone Lysyl Residues in Vivo—To investigate histone lysyl hydroxylation *in vivo*, we performed the amino acid composition analysis for analyzing a mixture of histone H2A/H2B and a mixture of histone H3/H4 proteins isolated from two JMJD6 wild-type and two JMJD6 knock-out whole embryos at E14.5 (Fig. 4*A*). JMJD6 knock-out was confirmed by qRT-PCR and Western blotting (Fig. 4, *B* and *C*). The results showed that 0.097 and 0.080% of total lysyl residues in histone H2A/H2B and 0.094 and 0.046% of those in histone H3/H4 were 5-hydroxylated in each of the two JMJD6 wild-type mice (Fig. 4, *D* and *E*), whereas 0.004 and 0.011% of total lysyl residues in histone H2A/H2B and 0.000 and 0.000% of those in histone H3/H4 were 5-hydroxylated in each of the two JMJD6 knock-out mice (Fig. 4, *D* and *E*), indicating that JMJD6 hydroxylates histone lysyl residues *in vivo*.

We also generated Dox-inducible JMJD6 stable HEK293 cells. JMJD6 induction by Dox was confirmed by qRT-PCR and Western blotting (Fig. 5, *A* and *B*) and increased 5-hydroxylation levels of histone lysyl residues (Fig. 5*C*). In addition, we purified histones from a 6-month-old JMJD6 wild-type mouse

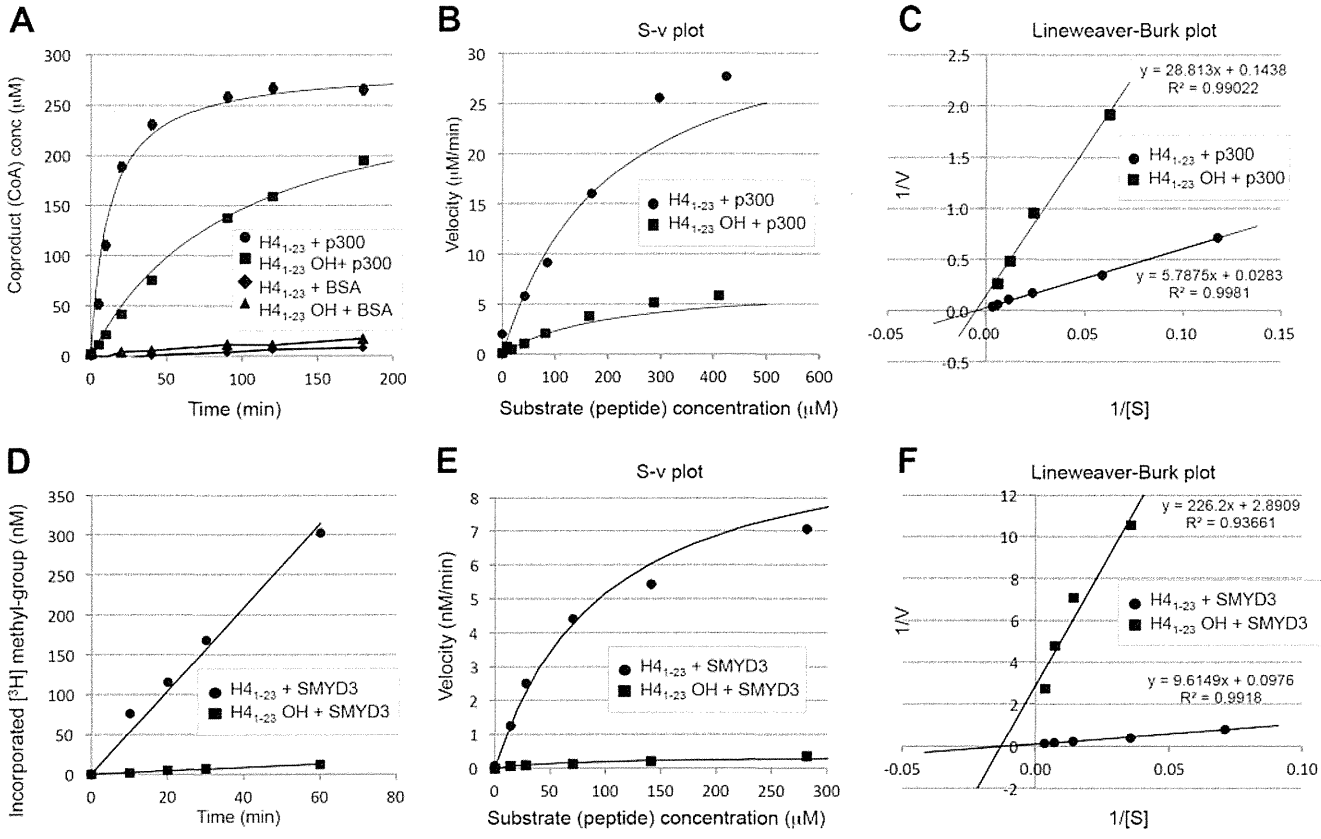

FIGURE 6. **5-Hydroxylation of lysyl residue impairs *N*-acetylation and *N*-methylation *in vitro*.** *A–C*, the *in vitro* colorimetric HAT assay was performed using a fixed amount of p300 (0.44 μM) and control $H4_{1-23}$ peptides (●) or 5-hydroxylysine-containing peptides ($H4_{1-23}$ OH, ■). BSA was used as a negative control (◆, ▲). After the reactions, absorbance (405 nm) of the coproduct (CoA) was measured. *A*, reactions were terminated at the indicated time points, and the concentration of CoA was calculated on the basis of a standard curve that was generated from β2-mercaptoethanol. *B* and *E*, substrate concentration-velocity (s-v) plot. *C* and *F*, Lineweaver-Burk plot. The *vertical axis* is 1/velocity [v], and the *horizontal axis* is 1/substrate concentration [S]. *D–F*, the *in vitro* histone methyltransferase assay was performed using a fixed amount of SMYD3 (1 μM) and control $H4_{1-23}$ peptides (●) or 5-hydroxylysine-containing peptides ($H4_{1-23}$OH, ■). AdoMet was used as a methyl donor. After the reactions, radioactivity (cpm) of the ^{3}H-methylated substrates was measured. The concentration of incorporated ^{3}H-methyl groups (nM) was calculated based on the basis of radioactivity (1 cpm was 0.02563 nM in the reaction). *D*, reactions were performed with fixed amounts of the peptides (141 μM) and terminated at the indicated time points.

testis, which expressed JMJD6 at the highest level among various tissues and cells (Fig. 5, *D* and *E*). In the testis, 0.238 and 0.054% of total lysyl residues in histone H2A/H2B and H3/H4, respectively, were 5-hydroxylated (Fig. 5*F*). In the mouse J1 ES cells, 0.053 and 0.020% of total lysyl residues in histone H2A/H2B and H3/H4, respectively, were 5-hydroxylated (Fig. 5*F*).

5-Hydroxylation Prevents N-Acetylation and N-Methylation of Histone Lysyl Residues in Vitro—Because lysyl residues in histone tails are often subjected to *N*-acetylation and *N*-methylation, we examined whether 5-hydroxylation of lysyl residues affects modifications at the ϵ-amino groups. First, we examined the effect of lysyl 5-hydroxylation on histone H4 *N*-acetylation by p300, which catalyzes *N*-acetylation of the ϵ-amino group of lysyl residues, including histone H4K5 and H4K8, through its HAT domain (12). Kinetic analysis using the unmodified and the 5-hydroxylysine containing $H4_{1-23}$ peptides in which all the lysines were substituted with 5-hydroxylysines as substrates revealed that 5-hydroxylation largely interfered with the HAT activity of p300 *in vitro* (Fig. 6, *A–C*). Lineweaver-Burk plot analysis was performed to calculate the maximum velocity (V_{max}) and Michaelis constant (K_m) values (Table 1; Fig. 6*C*, $R^2 = 0.9981$ and 0.9902). V_{max} of the reactions in which p300 acetylated the 5-hydroxylysine-containing peptides ($H4_{1-23}$OH) was 5-fold less than that of the control peptides (6.95 ± 0.45 and 35.34 ± 1.65 μM/min, respectively), whereas K_m of the two reactions was quite similar (204.51 ± 10.12 and 200.37 ± 14.32 μM, respectively), indicating that 5-hydroxylation does not inhibit binding of lysyl residues to p300 but reduces the catalytic efficiency.

TABLE 1

Effect of 5-hydroxylation on *N*-acetylation of ϵ-amino group of lysyl residues

Lineweaver-Burk plots were used for estimation of the kinetic constants, V_{max}, and K_m. R^2 is the determination coefficient (see Fig. 6*C*).

	V_{max}	K_m
	μM/min	μM
$H4_{1-23}$ + p300	35.34 ± 1.65 (R^2 = 0.9981)	204.51 ± 10.12
$H4_{1-23}$ OH + p300	6.95 ± 0.45 (R^2 = 0.9902)	200.37 ± 14.32

TABLE 2

Effect of 5-hydroxylation on *N*-methylation of ϵ-amino group of lysyl residues

Lineweaver-Burk plots were used for estimation of the kinetic constants, V_{max}, and K_m. R^2 is the determination coefficient (see Fig. 6*F*).

	V_{max}	K_m
	nM/min	
$H4_{1-23}$ + SMYD3	10.90 ± 0.92 (R^2 = 0.9918)	80.63 ± 16.26 μM
$H4_{1-23}$ OH + SMYD3	0.48 ± 0.26 (R^2 = 0.9366)	75.26 ± 9.60 μM

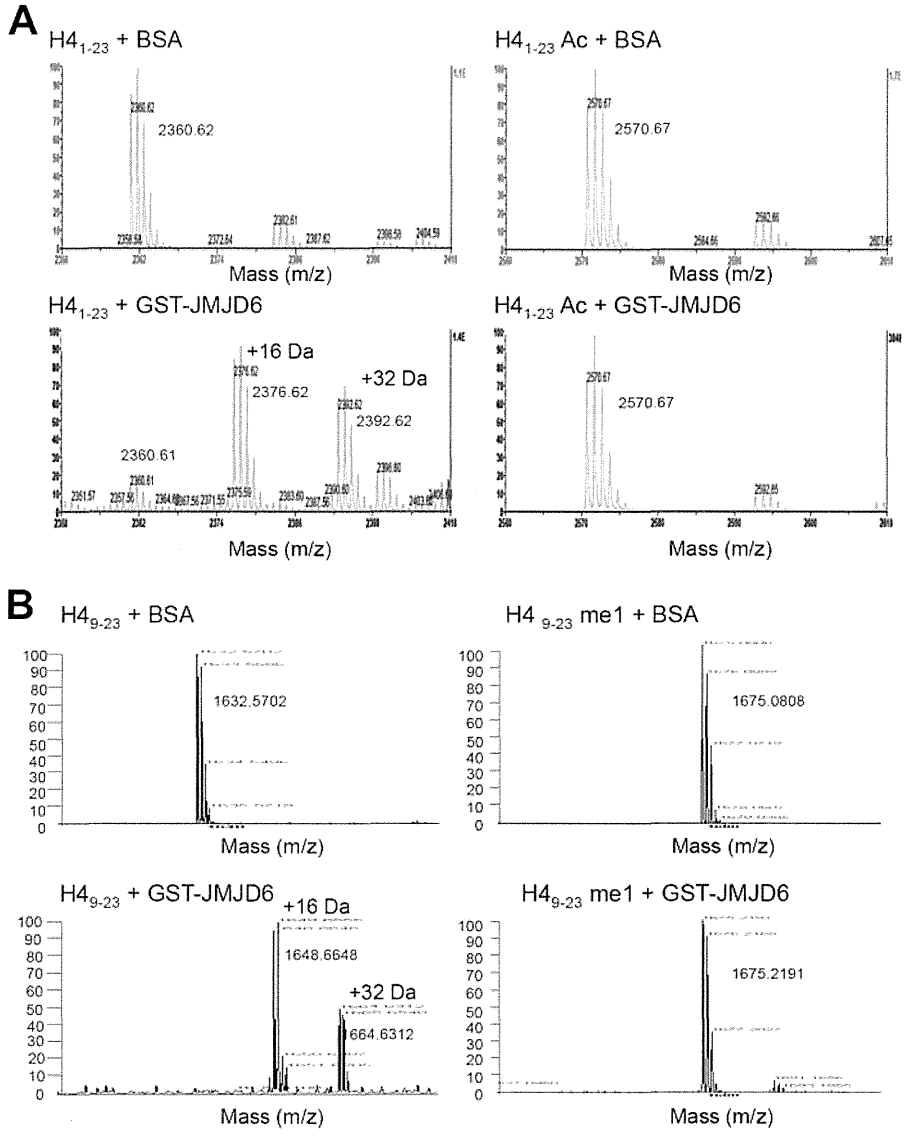

FIGURE 7. ***N*-Acetylation and *N*-methylation of lysyl residues impairs 5-hydroxylation by JMJD6 *in vitro*.** *A*, the *in vitro* hydroxylation assay was performed using GST-JMJD6 (10 μM) and 85 μM of control $H4_{1-23}$ peptides or *N*-acetyl-lysine-containing peptides. *B*, the *in vitro* hydroxylation assay was performed using GST-JMJD6 (10 μM) and 85 μM control $H4_{1-23}$ peptides or *N*-monomethyl-lysine-containing peptides. BSA was used as a negative control. 5-Hydroxylation by JMJD6 was detected by MS analysis.

We also examined the effect of lysyl 5-hydroxylation on the histone methyltransferase activity of SMYD3, which catalyzes lysyl *N*-methylation of histone H3 (13) and also H4 (data not shown) through its SET (su(var) 3–9 enhancer-of-zeste trithorax) domain by the histone methyltransferase assay. The results showed that 5-hydroxylation at lysyl residues almost completely inhibited *N*-methylation catalyzed by SMYD3 (Table 2 and Fig. 6, *D–F*); V_{max} values of the reactions with the control peptides ($H4_{1-23}$) and the 5-hydroxylysine-containing peptides ($H4_{1-23}OH$) as substrates were 10.90 ± 0.92 and 0.48 ± 0.26 nM/min, respectively. Similar to the HAT assay, K_m values of the two reactions were ~80.63 ± 16.26 and 75.26 ± 9.60 μM, respectively.

Subsequently, we performed reciprocal experiments using $H4_{1-23}$ or $H4_{9-23}$ peptides, in which all the lysines are either unmodified, *N*-acetylated, or *N*-monomethylated. JMJD6 effectively hydroxylated the control peptides (Fig. 7, *A* and *B*, *left panels*); however, *N*-acetylation and *N*-monomethylation at the ϵ-amino group of the lysines completely blocked 5-hydroxylation by JMJD6 (Fig. 7, *A* and *B*, *right panels*).

DISCUSSION

We found a novel histone modification, 5-hydroxylation, by JMJD6. JMJD6 reportedly hydroxylates a splicing factor, U2AF65 (1). That study and another report (1, 14) stated that evidence of histone lysyl hydroxylation was not found by MS-based analysis *in vivo*. In the present study, we developed an alternative method, amino acid composition analysis, to detect 5-hydroxylation of histone lysyl residues. As reported previously, we have not detected clear evidence of 5-hydroxylation of histone lysyl residues by MS-based analysis. We think that there are several causes for this. 1) The amount of 5-hydroxylysine is too small to detect by MS-based analysis. 2) Artificial methionine oxidation during preparation of samples for MS analysis

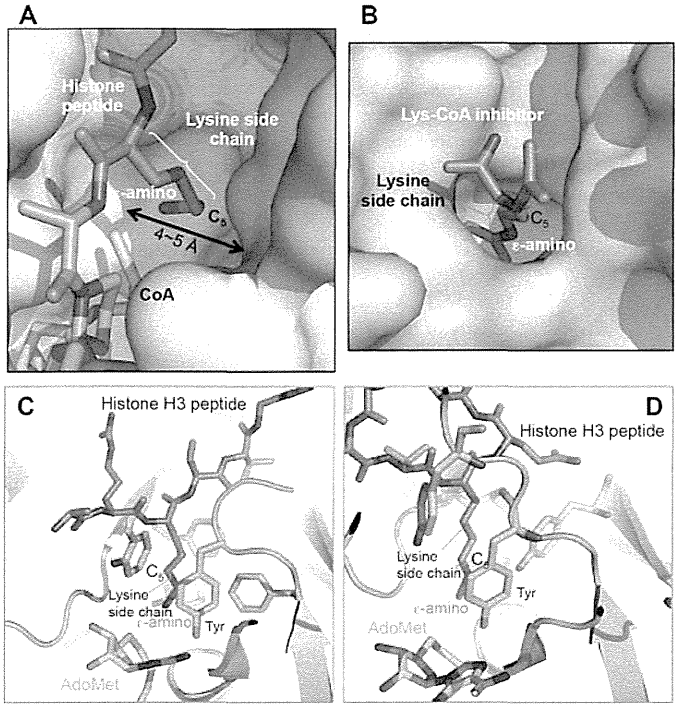

FIGURE 8. **Structure around the active site of HAT domains and SET domains, a lysine side chain, and an *S*-adenosyl methionine (*AdoMet*).** *A*, spatial localization among the HAT domain of GCN5 (*gray*), a lysine side chain (*magenta*), and CoA (*cyan*) (Protein Data Bank code 1QSN). The 5-hydroxyl group may locate close to acetyl-CoA, indicating that this may work as a steric barrier and prevent effective *N*-acetylation by the catalytic domain. *B*, structure of the HAT domain of p300 (*gray*) in complex with inhibitor, Lys-CoA (*magenta*) (Protein Data Bank code 3BIY). The 5-hydroxyl group may restrict the conformation of lysine side chain in the catalytic pocket of p300. The figures were prepared by using program PyMOL. *C*, spatial localization among the SET domain of *N. crassa* Dim-5 (*green*), a histone H3 peptide (*magenta*), and AdoMet (*cyan*) (Protein Data Bank code 1PEG). *D*, spatial association among the SET domain of human SETD7/9 (*green*), a histone H3 peptide containing monomethylated Lys-4 (*magenta*), and AdoMet (*cyan*) (Protein Data Bank code 1O9S). A side chain of a lysine residue locates in tightly hydrophobic pocket of the SET domains (*C* and *D*). Hydroxylation at position C_5 of the chain may prevent a lysine side chain to locate in the pocket, causing inhibition of *N*-methylation by SET domains.

makes detection of 5-hydroxylysine difficult. 3) 5-Hydroxylysine could be an intermediate form as it is in collagen, and a further unknown modification(s) such as glycosylation could be added; the final product of collagen is glucosylgalactosyl hydroxylysine (4). The collagen hydroxylase, PLOD3, possesses galactosyltransferase and glucosyltransferase activities. Unlike PLOD3, JMJD6 does not appear to possess any other enzymatic activities by domain search; therefore, it is difficult to assume possible further modification(s) by its protein structure. We may have been able to detect 5-hydroxylation in histone lysyl residues by amino acid composition analysis but not by the MS-based analysis because many modifications such as glycosylation or galactosylation could be removed during the hydrolysis process of amino acid composition analysis. By this analysis, we detected both *SS*/*RR*- and *SR*/*RS*-hydroxylysine in JMJD6-treated histone peptides and also in JMJD6 wild-type E14.5 embryos, ES cells, and the Dox-inducible JMJD6 stable HEK293 cells. Because the relationship between *RR* and *RS* and also between *SS* and *RS* is a diastereomer, we were able to distinguish them. However, because a relationship between *SS* and *RR*, and also between *RS* and *SR* is an enantiomer, we were not able to separate them by this method. Despite this, these two peaks are most likely *SS*- and *RS*-hydroxylysine because JMJD6 is reported to generate *SS*-hydroxylysine (11). The *RS*-hydroxylysine could be generated from *SS*-hydroxylysine through the lactone derivative, 3-amino-6-(aminomethyl)oxan-2-one, which is unstable and difficult to be quantified. Because of this difficulty, we only quantified *SS*/*RR*- and *RS*/*SR*-hydroxylysine in this report. Therefore, actual quantity of 5-hydroxylysine in the samples examined here could be a little higher.

Because we detected 5-hydroxylysines in the UHRF1 KO ES cells (data not shown), UHRF1 is not required for 5-hydroxylation of histone lysyl residues by JMJD6. Therefore, biological significance of the interaction between UHRF1 and JMJD6 remains unclear. Further analysis is also required to determine the biological significance of 5-hydroxylation of histone lysyl residues. *In vitro* experiments suggest that 5-hydroxylation can inhibit *N*-acetylation and *N*-methylation by p300 and SMYD3. The active site structure of the p300 and general control of amino acid synthesis 5 (GCN5) HAT domains showed that the side chain of the 5-hydroxylysine can invade the catalytic pocket; however, the 5-hydroxyl group may disturb active form formation of the substrate (Fig. 8, *A* and *B*). The catalytic site of SET domains of *Neurospora crassa* Dim-5 and human SETD7, which are structurally similar to SMYD3 (15), suggested that the side chain of 5-hydroxylysine can invade the catalytic pocket; however, the 5-hydroxyl group may disturb an active form formation of the substrate (16, 17) similar to that in HAT domains (Fig. 8, *C* and *D*). Therefore, 5-hydroxylation could be important in the context of the histone code. It is known that histones H2A and H2B move more dynamically between the nucleosome and nucleoplasm. 5-Hydroxylation of these histones may have some effects for the movement because the modification was detected more in histones H2A/H2B than in histones H3/H4. The expression pattern of JMJD6 is also interesting. JMJD6 may play important role(s) in the testis, such as a role in histone-protamine exchange. We believe that our present finding provides a novel insight into epigenetic regulations of gene transcription and/or chromosomal rearrangement.

Acknowledgments—We thank Dr. Haruhiko Koseki and Dr. Jafar Sharif for providing us UHRF1 KO ES cells; Professor Shoji Tajima, Dr. Isao Suetake, Dr. Yoichi Shinkai, Dr. Kenji Ichiyanagi, Dr. Fumiyuki Sanematsu, and Dr. Hyun-Soo Cho for useful advice; and Yuichi Mishima and Dr. Atsuhiko Toyama for technical assistance.

REFERENCES

1. Webby, C. J., Wolf, A., Gromak, N., Dreger, M., Kramer, H., Kessler, B., Nielsen, M. L., Schmitz, C., Butler, D. S., Yates, J. R., 3rd, Delahunty, C. M., Hahn, P., Lengeling, A., Mann, M., Proudfoot, N. J., Schofield, C. J., and Böttger, A. (2009) Jmjd6 catalyses lysyl-hydroxylation of U2AF65, a protein associated with RNA splicing. *Science* **325,** 90–93
2. Hong, X., Zang, J., White, J., Wang, C., Pan, C. H., Zhao, R., Murphy, R. C., Dai, S., Henson, P., Kappler, J. W., Hagman, J., and Zhang, G. (2010) Interaction of JMJD6 with single-stranded RNA. *Proc. Natl. Acad. Sci. U.S.A.* **107,** 14568–14572
3. Loenarz, C., and Schofield, C. J. (2008) Expanding chemical biology of 2-oxoglutarate oxygenases. *Nat. Chem. Biol.* **4,** 152–156
4. Myllylä, R., Wang, C., Heikkinen, J., Juffer, A., Lampela, O., Risteli, M., Ruotsalainen, H., Salo, A., and Sipilä, L. (2007) Expanding the lysyl hydrox-

ylase toolbox: new insights into the localization and activities of lysyl hydroxylase 3 (LH3). *J. Cell. Physiol.* **212,** 323–329
5. Shi, Y., and Whetstine, J. R. (2007) Dynamic regulation of histone lysine methylation by demethylases. *Mol. Cell* **25,** 1–14
6. Kunisaki, Y., Masuko, S., Noda, M., Inayoshi, A., Sanui, T., Harada, M., Sasazuki, T., and Fukui, Y. (2004) Defective fetal liver erythropoiesis and T lymphopoiesis in mice lacking the phosphatidylserine receptor. *Blood* **103,** 3362–3364
7. Böse, J., Gruber, A. D., Helming, L., Schiebe, S., Wegener, I., Hafner, M., Beales, M., Köntgen, F., and Lengeling, A. (2004) The phosphatidylserine receptor has essential functions during embryogenesis but not in apoptotic cell removal. *J. Biol.* **3,** 15
8. Unoki, M., Brunet, J., and Mousli, M. (2009) Drug discovery targeting epigenetic codes: the great potential of UHRF1, which links DNA methylation and histone modifications, as a drug target in cancers and toxoplasmosis. *Biochem. Pharmacol.* **78,** 1279–1288
9. Masuda, A., and Dohmae, N. (2010) Automated Protein Hydrolysis Delivering Sample to a Solid Acid Catalyst for Amino Acid Analysis. *Anal. Chem.* **82,** 8939–8945
10. Strahl, B. D., Ohba, R., Cook, R. G., and Allis, C. D. (1999) Methylation of histone H3 at lysine 4 is highly conserved and correlates with transcriptionally active nuclei in *Tetrahymena*. *Proc. Natl. Acad. Sci. U.S.A.* **96,** 14967–14972
11. Mantri, M., Loik, N. D., Hamed, R. B., Claridge, T. D., McCullagh, J. S., and Schofield, C. J. (2011) The 2-oxoglutarate-dependent oxygenase JMJD6 catalyses oxidation of lysine residues to give 5S-hydroxylysine residues. *Chembiochem.* **12,** 531–534
12. Schiltz, R. L., Mizzen, C. A., Vassilev, A., Cook, R. G., Allis, C. D., and Nakatani, Y. (1999) Overlapping but distinct patterns of histone acetylation by the human coactivators p300 and PCAF within nucleosomal substrates. *J. Biol. Chem.* **274,** 1189–1192
13. Hamamoto, R., Furukawa, Y., Morita, M., Iimura, Y., Silva, F. P., Li, M., Yagyu, R., and Nakamura, Y. (2004) SMYD3 encodes a histone methyltransferase involved in the proliferation of cancer cells. *Nat. Cell Biol.* **6,** 731–740
14. Han, G., Li, J., Wang, Y., Li, X., Mao, H., Liu, Y., and Chen, C. D. (2012) The hydroxylation activity of Jmjd6 is required for its homo-oligomerization. *J. Cell. Biochem.* **113,** 1663–1670
15. Dillon, S. C., Zhang, X., Trievel, R. C., and Cheng, X. (2005) The SET-domain protein superfamily: protein lysine methyltransferases. *Genome Biol.* **6,** 227
16. Zhang, X., Tamaru, H., Khan, S. I., Horton, J. R., Keefe, L. J., Selker, E. U., and Cheng, X. (2002) Structure of the Neurospora SET domain protein DIM-5, a histone H3 lysine methyltransferase. *Cell* **111,** 117–127
17. Subramanian, K., Jia, D., Kapoor-Vazirani, P., Powell, D. R., Collins, R. E., Sharma, D., Peng, J., Cheng, X., and Vertino, P. M. (2008) Regulation of estrogen receptor α by the SET7 lysine methyltransferase. *Mol. Cell* **30,** 336–347

OPEN ACCESS Freely available online

PLOS | ONE

Hepatitis C Virus Translation Preferentially Depends on Active RNA Replication

Helene Minyi Liu[1], Hideki Aizaki[1], Keigo Machida[1], J.-H. James Ou[1], Michael M. C. Lai[1,2]*

1 Department of Molecular Microbiology and Immunology, Keck School of Medicine, University of Southern California, Los Angeles, California, United States of America, **2** Institute of Molecular Biology, Academia Sinica, Nankang, Taipei, Taiwan

Abstract

Hepatitis C virus (HCV) RNA initiates its replication on a detergent-resistant membrane structure derived from the endoplasmic reticulum (ER) in the HCV replicon cells. By performing a pulse-chase study of BrU-labeled HCV RNA, we found that the newly-synthesized HCV RNA traveled along the anterograde-membrane traffic and moved away from the ER. Presumably, the RNA moved to the site of translation or virion assembly in the later steps of viral life cycle. In this study, we further addressed how HCV RNA translation was regulated by HCV RNA trafficking. When the movement of HCV RNA from the site of RNA synthesis to the Golgi complex was blocked by nocodazole, an inhibitor of ER-Golgi transport, HCV protein translation was surprisingly enhanced, suggesting that the translation of viral proteins occurred near the site of RNA synthesis. We also found that the translation of HCV proteins was dependent on active RNA synthesis: inhibition of viral RNA synthesis by an NS5B inhibitor resulted in decreased HCV viral protein synthesis even when the total amount of intracellular HCV RNA remained unchanged. Furthermore, the translation activity of the replication-defective HCV replicons or viral RNA with an NS5B mutation was greatly reduced as compared to that of the corresponding wildtype RNA. By performing live cell labeling of newly synthesized HCV RNA and proteins, we further showed that the newly synthesized HCV proteins colocalized with the newly synthesized viral RNA, suggesting that HCV RNA replication and protein translation take place at or near the same site. Our findings together indicate that the translation of HCV RNA is coupled to RNA replication and that the both processes may occur at the same subcellular membrane compartments, which we term the replicasome.

Citation: Liu HM, Aizaki H, Machida K, Ou J-HJ, Lai MMC (2012) Hepatitis C Virus Translation Preferentially Depends on Active RNA Replication. PLoS ONE 7(8): e43600. doi:10.1371/journal.pone.0043600

Editor: Jinah Choi, University of California Merced, United States of America

Received May 30, 2012; **Accepted** July 26, 2012; **Published** August 24, 2012

Funding: This work was supported by National Institutes of Health grants AI40038, CA108302, and Academia Sinica Institutional Fund. No additional external funding received for this study. The funders had no role in study design, data collection and analysis, decision to publish, or preparation of the manuscript.

Competing Interests: The authors have declared that no competing interests exist.

* E-mail: michlai@gate.sinica.edu.tw

Introduction

Hepatitis C virus (HCV) is a positive-sense RNA virus that is estimated to chronically infect as many as 3% of the world's population. As a member of Flaviviridae, HCV is an enveloped virus with a single, positive-stranded RNA around 9.6 kb in length [1]. The viral genome encodes a large viral polyprotein, which is proteolytically processed by cellular signal peptidases and viral proteases into structural (C, E1, E2, and p7) and non-structural (NS2, NS3, NS4A, NS4B, NS5A and NS5B) proteins [2]. Membrane association of the viral proteins is essential for HCV replication, at both steps of RNA transcription and translation [3–5]. To decipher the mechanisms by which HCV navigates these steps may necessitate an understanding of the cell biological processes as diverse as cytoplasmic organelle structure and membrane biogenesis and trafficking in the secretory pathway.

Using the HCV subgenomic replicon system as well as infectious virus system, many host factors have been identified to be involved in HCV RNA replication, including the human homologue of the 33-kDa vesicle-associated membrane protein-associated protein (hVAP-33) [6], Golgi-specific brefeldin A resistant guanine nucleotide exchange factor 1(GBF1) [7], Endocytic Rab proteins [8], polypyrimidine-tract-binding protein (PTB) [9,10], La autoantigen [10], SYNCRIP [11], and host geranylgeranylated proteins and fatty acids [12]. These host proteins that are identified to be in the HCV RNA replication complexes are important in either membrane sorting and trafficking or RNA binding and processing. Some of these host factors, such as PTB and La autoantigen, have been found to regulate HCV translation as well_ENREF_13 by virtue of their binding to the 5′ or 3′ UTR of HCV RNA [13–15]. The identification of host proteins with dual-functions in regulating both translation and transcription implies the possibility of coupled transcription/translation of HCV RNA.

The balance between viral RNA transcription and translation is critical for the replication of positive-stranded RNA viruses, since the same RNA is used both for translation and as the template for negative-strand RNA synthesis. Transcription of poliovirus has been reported to be dependent on the translational activity of the viral RNA [16]. On the other hand, the translation of Sindbis virus and vesicular stomatitis virus has been reported to be transcriptionally dependent [17]. Such coupling of transcription-translation has been well documented to confer advantage in maintaining the stability of the RNA molecule in bacteria [18,19] and also to respond to regulatory signals coordinately.

In this study, we observed that HCV RNA exit from the site of RNA synthesis to the Golgi complex, a process that can be blocked by nocodazole, an inhibitor of the ER-Golgi transport pathway. Surprisingly, HCV protein translation was enhanced when HCV RNA movement was blocked, suggesting that the translation of

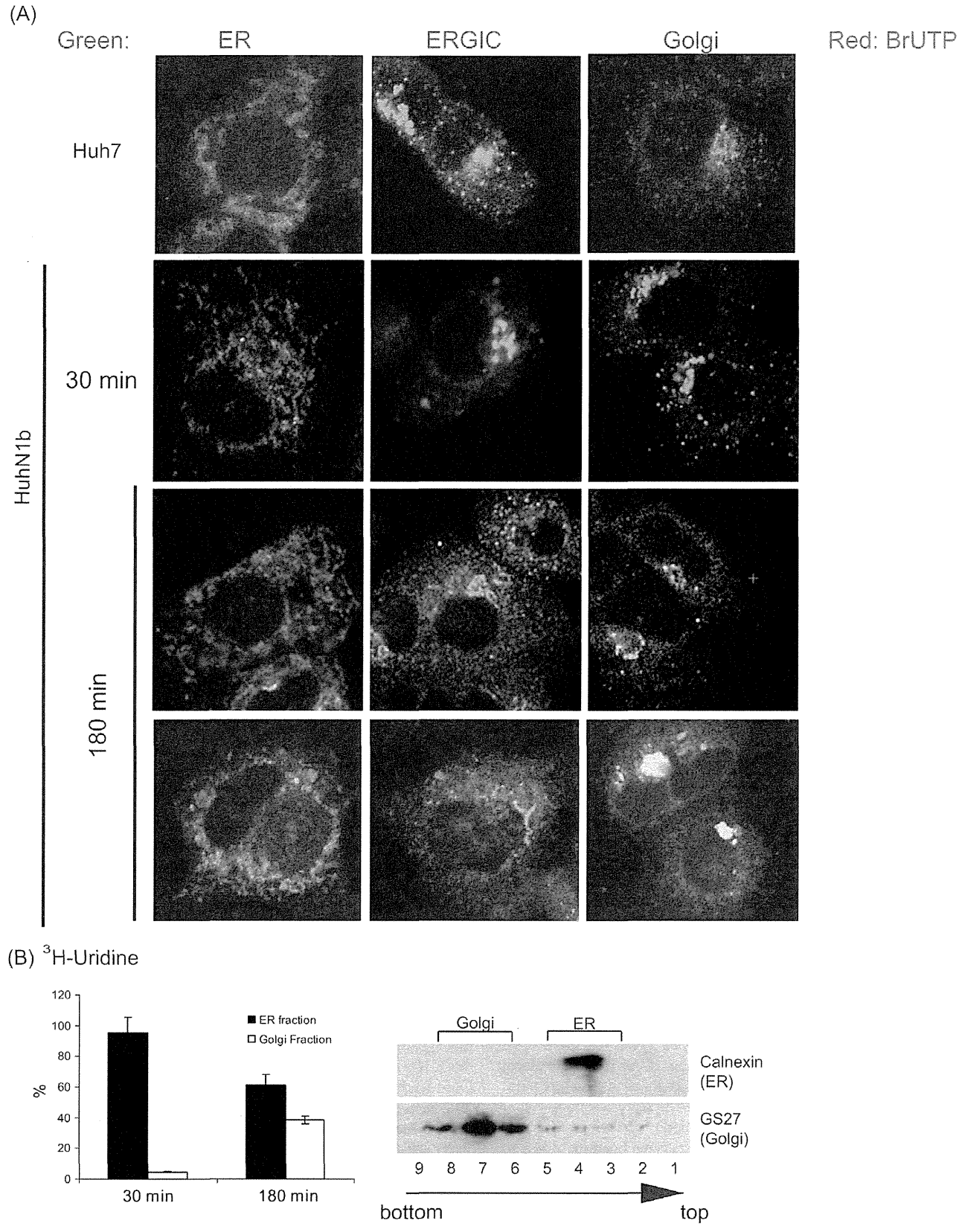

Figure 1. The translocation of newly-synthesized HCV RNA. HCV replicon cells were labeled with BrUTP (A) or ^{3}H-Uridine (B) in the presence of actinomycin D and chased for up to 180 minutes. (A) Immunofluorescence staining with anti-BrdU and other organelle antibodies shows the colocalization of BrU-labeled HCV RNA with ER initially (30 min) and then with Golgi (180 min). (B) Fractionation of ER and Golgi by sucrose gradient.

Fraction numbers and their gradient positions are noted at the bottom. ^{3}H-Uridine-labeled RNA in the ER (fraction 4) and the Golgi (fraction 6–8) fractions were collected, and the radioactivity of ^{3}H-Uridine-labeled RNA was counted. Immunoblotting of ER and Golgi makers demonstrates the separation of ER and Golgi by sucrose gradient fractionation.
doi:10.1371/journal.pone.0043600.g001

viral proteins occurred near the site of RNA synthesis. We also found that the translation of HCV proteins was dependent on active RNA synthesis: inhibition of RNA synthesis resulted in decreased HCV viral protein synthesis before there was significant decrease in the total amount of HCV RNA, and that the replication-defective HCV RNA could not be translated efficiently *in vivo*. Finally, we found that at least most of the newly synthesized HCV proteins colocalized with the newly synthesized viral proteins. These findings together thus indicate that HCV replication and translation are coupled, in the sense that replication of viral RNA is linked to translation of viral RNA in situ.

Materials and Methods

Cell Lines, HCV Full-length and Subgenomic Constructs

Huh7 or Huh7.5 cells were grown at 37°C in Dulbecco's modified Eagle medium (DMEM) supplemented with 10% fetal bovine serum (FBS) and nonessential amino acids. Huh7 cells were obtained from Dr. Sato's lab [20], and Huh7.5 cells were obtained from Dr. Rice' lab [21]. Bicistronic HCV-N1b replicon was derived from the HCV-N strain with a neomycin-phosphotransferase (NPT) gene for selection as described [22]. Huh-Noe cells are stable cells derived from Huh7 cells with NPT expression as described previously [23,24]. Huh-N1b replicon cell line and Huh-Neo cells containing an NPT gene were grown under the same conditions as Huh7 cells using the same media containing 0.5 mg/ml G418.

In vitro Transcription and Electroporation of HCV Full-length and Subgenomic RNA

HCV JFH1 and JFH-GND constructs were obtained from Dr. Wakita's lab (NIID, Japan) [25]. Bicistronic replicon with either firefly luciferase (FFLuc) or Renilla luciferase (RLuc) gene was derived from HCV1bneo [22] by replacing NPT with either FFLuc or RLuc reporter gene. To prepare the template for *in vitro* transcription, the plasmids were digested by Xba I and Mungbean nuclease and gel-purified. For electroporation, Huh7 or Huh7.5 cells were trypsinized, washed and resuspended in serum-free DMEM. HCV replicon RNA or JFH full-length RNA were transcribed *in vitro* by T7 MegaScript (Ambion). A total of 6 to 10 μg of RNA and 10^{7} Huh7 cells were mixed and incubated on ice for 5 minutes and subjected to an electric pulse at 975 μF and 220 V. Cells were immediately transferred to 8 ml of DMEM containing 10% FBS for incubation.

Labeling and Immunofluorescene Staining of De Novo-synthesized Viral RNA and Newly-translated Peptides

Labeling of de novo-synthesized viral RNA, immunofluorescence staining and confocal microscopy were modified from the previously described methods [26]. Briefly, Huh7, Huh7.5 or replicon cells were plated on 8-well chamber slides at density of 1×10^{4} cells per well. Two days after seeding, cells were incubated with actinomycin D (10 μg/ml) for 1 hour to inhibit cellular RNA synthesis, and in some experiments, also with 20 nM of hippuristanol [27] for 1 hour to inhibit eIF4A-dependent protein synthesis, which represents most of the host cell protein synthesis. For immunofluorescence detection of de novo synthesized viral RNA, 2 mM of bromouridine triphosphate (BrUTP) was subsequently transfected into cells at 4°C for 15 min using Fugene 6 transfection reagent according to the manufacturer's instructions (Roche). For live-cell imaging of both RNA and proteins, Cy5-UTP and BODIPY-FL-Lys-tRNA were cotransfected to label nascent HCV RNA and peptides, respectively. For immunofluorescence staining of both nascent viral RNA and proteins, Transcend biotinyl-Lys-RNA (Promega) [28] and BrUTP were instead used. The transfected cells were washed with phosphate-buffered saline (PBS) twice and incubated at 37°C with DMEM supplemented with 10% FBS for different periods of time. After incubation, cells were washed twice with PBS and subsequently fixed with 4% formaldehyde for 1 hr at 4°C. For permeabilization, the cells were treated with 0.1% Triton X-100 in PBS supplemented with 1% FBS for 30 min at RT. Primary antibodies were diluted in PBS containing 1% bovine serum albumin (BSA) and incubated with cells for 1 hr at RT. After three washes in PBS, the cells were incubated with fluorescein-isothiocyanate (FITC)-conjugated or Rhodamine-conjugated secondary antibodies, or Texas-red-conjugated streptoavidin diluted at a 1:100 with PBS containing 5% BSA for 1 hr at RT. Then the cells were washed three times in PBS and mounted in Vectashield (Vector Laboratories).

Analysis of Intracellular Viral RNA by Northern Blotting and Real-time RT PCR

To determine the quantity of RNA by real-time PCR, a single-tube reaction was performed by using the TaqMan EZ RT-PCR Core Reagents (Applied Biosystems). Duplicate reactions for RNA standards and the samples were performed in 20-μl volume using 1 μl of HCV RNA, primers from HCV 5′ non-coding region (5′ GAG TGT CGT GCA GCC TCC A 3′ and 5′ CAC TCG CAA GCA CCC TAT CA 3′) of the HCV 1b sequence [29], and a fluorescent probe [5′ (FAM) CCC GCA AGA CTG CTA GCC GAG TAG TGT TGG (TAMRA) 3′] spanning these two regions. The RT step was performed at 60°C for 50 min, followed by 1 min at 50°C. The amplification condition was as follows: 95°C for 5 min and 50 cycles of denaturation at 94°C for 15 sec, annealing at 55°C for 10 sec, and extension at 69°C for 1 min.

Using the ABI Prism 7900 program, standard curves of the assays were obtained automatically by plotting the three hold values against each standard dilution of known concentration (10^{1}–10^{6} copies per reaction) of HCV genotype 1b transcript. The same software was used to calculate the coefficients of regression. Values were normalized to that of GAPDH (Applied Biosystems). Each test was done in triplicate and averages were obtained.

Fractionation of ER and Golgi Membrane

The procedure was based on the published method [30]. Cell lysates were applied to a discontinuous sucrose gradient composed of layers of 2 M, 1.3 M, 1.0 M and 0.6 M sucrose. The ER fraction was concentrated at the interface between 0.6 M and 1.0 M sucrose, and the Golgi fraction was concentrated at the interface between 2 M and 1.3 M. To determine the signal of ^{3}H-Uridine-labeled RNA, the fractions were passed through DE81 membranes to concentrate the labeled RNA. The membranes were then counted by scintillation counter, and the ratio of signals from the ER and Golgi fractions were calculated.

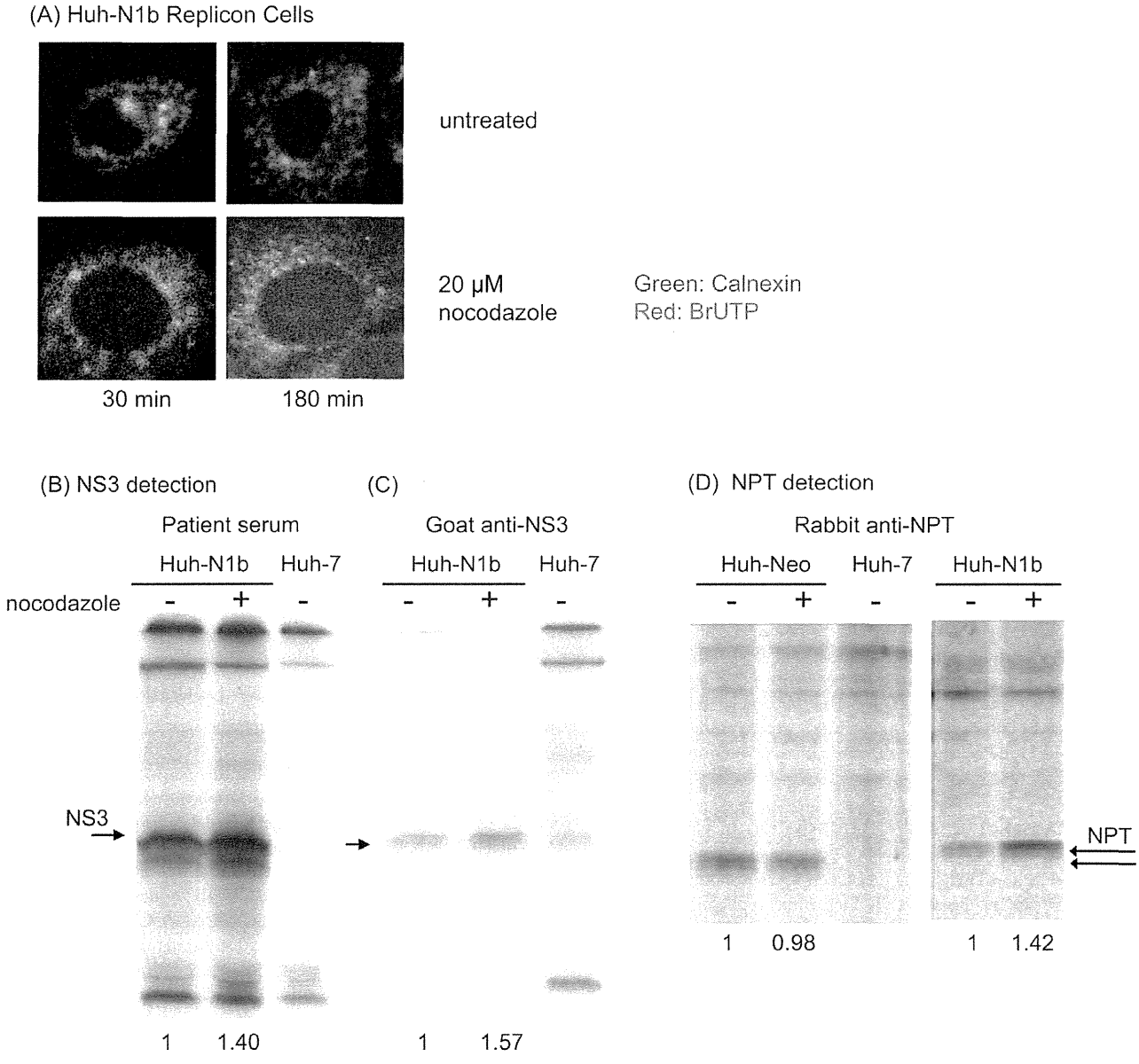

Figure 2. Increase in replicon RNA translation in nocodazole-treated HCV replicon cells. Huh-N1b cells was pre-treated with 20 μM nocodazole for 4 hours and then labeled with BrUTP or with ^{35}S-Methionine. (A) The BrU-labeled RNA remained colocalized with calnexin (an ER amrker) even after 180 min. (B–D) Proteins were immunoprecipitated with (B) HCV patient serum, (C) Goat anti-NS3 antibody, or (D) Rabbit anti-NPT antibody. The immunoprecipitated products were detected by autoradiography. The nocodazole-pretreated Huh-N1b cells showed about 50% increase in NS3 and NPT translated from replicon RNA, whereas NPT translation in the Huh-Neo control cells was not affected by the nocodazole treatment.
doi:10.1371/journal.pone.0043600.g002

Results

The Newly-synthesized HCV RNA Localizes to the ER and Moves Along with Anterograde Vesicle Trafficking

To visualize the replication of HCV RNA, we performed pulse BrUTP labeling in the actinomycin D-treated Huh-N1b replicon cells; under such conditions, only the viral RNA, which depends on RNA-dependent RNA polymerase, is labeled. After 15-minute labeling, the labeled RNA was chased in non-labeled media for 30 minutes to 3 hours, and the subcellular localization of BrU-labeled RNA was detected with anti-BrdU antibody and co-stained with individual organelle markers for ER (Calnexin), ERGIC (ER-GIC53), and Golgi apparatus (GS27), respectively (Fig. 1A). Consistent with our previous report, the newly synthesized HCV RNA was initially colocalized with the ER marker (Fig. 1A). However, after 3 hours of chase, the majority of the labeled HCV RNA did not colocalize with the ER marker, but colocalized with the Golgi marker instead (Fig. 1A, bottom panels). We did not observe any significant colocalization between BrU-labeled HCV RNA and ERGIC53. As a control, the BrUTP signals could not be detected in the actinomycin D-treated Huh7 cells, while the immunofluorescence-staining patterns of the ER, ERGIC, and Golgi apparatus appeared similar between Huh7 and Huh-N1b cells (Fig. 1A).

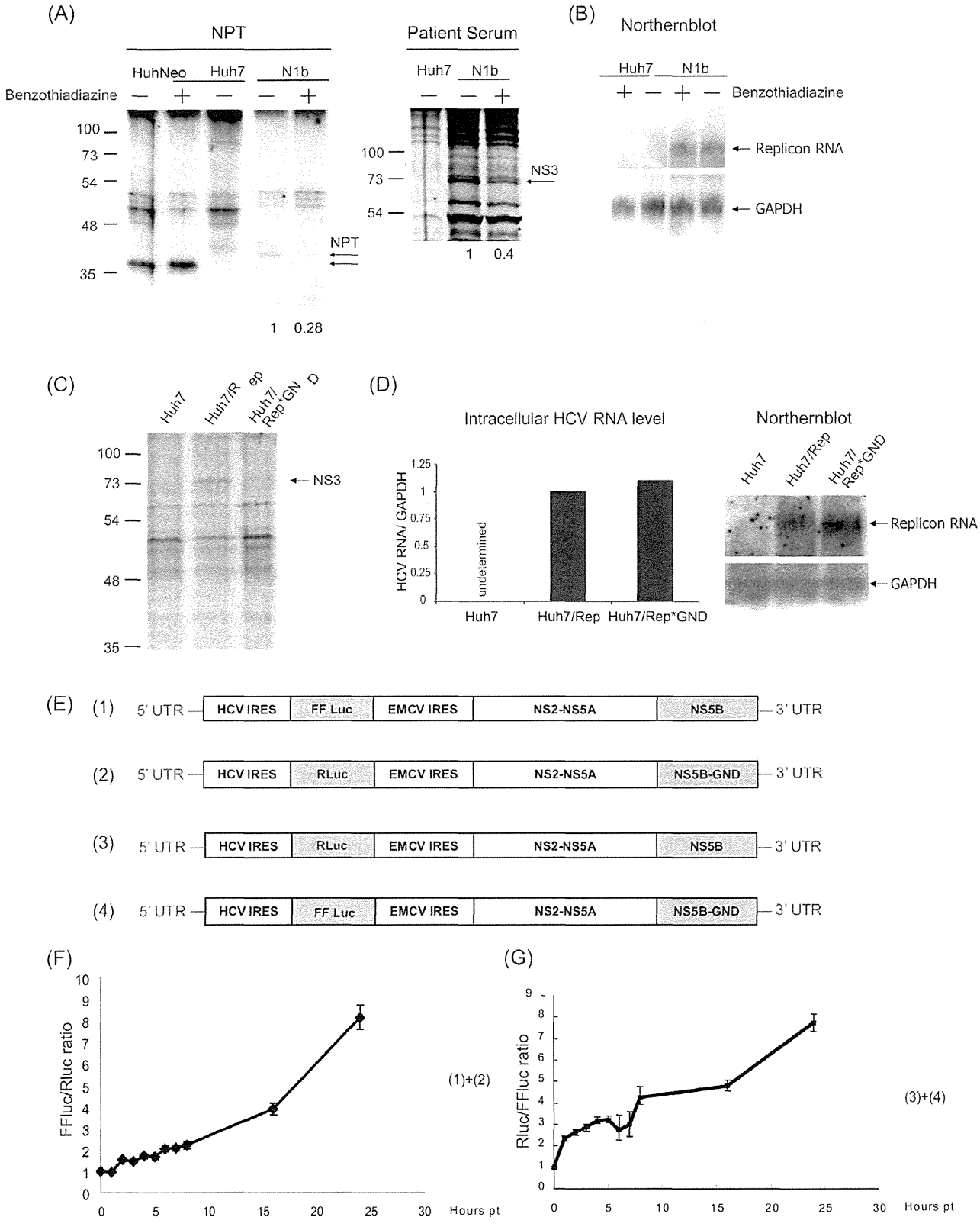

Figure 3. HCV RNA translation is dependent on the RNA transcription. (A), Mock- or Benzothiadiazine-treated Huh-N1b and Huh-Neo cells were labeled by ^{35}S-Methionine for 4 hours, and followed by immunoprecipitation with anti-NPT or anti-NS3 antibodies or sera from hepatitis C patients. The immunoprecipitates were separated by SDS-PAGE and detected by autoradiography. (B) The intracellular replicon RNA was detected by Northern blotting. (C) Huh7 cells transfected with *in vitro* transcribed Rep or the replication-defective Rep*GND RNA were metabolically labeled with ^{35}S-Methionine for 14 hours and followed by immunoprecipitation with anti-NS3 antibody. (D) The amounts of the intracellular HCV RNA in panel (C)

were determined by realtime RT-PCR and Nothern blotting. The relative ratios of the HCV RNA/GAPDH mRNA in the different cells are presented. E) Structures of the bi-cistronic replicon reporter constructs used. Time course studies of the luciferase activity in cells transfected with constructs 1 and 2 (panel (F)) and constructs 3 and 4 (panel (G)) were measured by dual luciferase assay at various time points after transfection. The ratios of the FFluc/Rluc (F) or Rluc/FFluc (G) are presented. Error bars represent +/− standard deviation.
doi:10.1371/journal.pone.0043600.g003

The ER-to-Golgi trafficking of the newly synthesized RNA was further confirmed by biochemical analysis. The actinomycin D-treated Huh-N1b cells were labeled with ^{3}H-uridine for 30 minutes and chased for 30 minutes to 3 hours. The labeled cell lysates were separated into ER and Golgi fractions by ultracentrifugation. Immunoblotting studies showed that the ER and the Golgi apparatus were efficiently separated by this procedure (Fig. 1B, right panel). The relative ratio of ^{3}H-uridine-labeled RNA in the Golgi and the ER significantly increased over time (Fig. 1B). The result suggested that the newly-synthesized HCV RNA was transported from the ER-derived to the Golgi apparatus-derived membranes.

HCV RNA Translation is Increased when Anterograde Vesicle Trafficking is Blocked

The ER-to-Golgi apparatus trafficking is known as the anterograde vesicle trafficking pathway, and can be blocked by nocodazole, which depolymerized microtubules and disrupts Golgi apparatus [31,32]. When BrUTP labeling was performed in the presence of nocodazole, BrU-labeled RNA colocalized with ER (calnexin) even after 3 hours of chase (Fig. 2A). Under these conditions, the morphology of cells was not altered by the treatment. These results suggest that the anterograde vesicle trafficking is involved in the transport of HCV RNA after its synthesis. We then further investigated if this transportation is required for certain steps of the HCV life cycle. Previously it has been shown that prolonged (more than 24 hours) nocodazole treatment inhibits HCV replication and viral production [33]; we thus tested if the nocodazole treatment could affect HCV translation. Huh7 or Huh-N1b (HCV replicon) cells were pre-treated with nocodazole for 4 hours, and then labeled with ^{35}S-Methionine for 4 hours to determine HCV translation activity (Fig. 2B). We determined the amounts of ^{35}S-Methionine-labeled Neomycin-phospho-transferase (NPT) and HCV NS3 proteins, both of which are encoded from the HCV replicon RNA but under the control of separate IRES elements. We found that after a 4-hour nocodazole treatment, the total amount of the labeled NS3 protein, as detected by anti-NS3 or HCV patients' sera, was significantly increased (Fig. 2, B and C). Similar observation was made for the NPT protein translated from the HCV replicon (Fig. 2D). Quantitation of the proteins showed a 40%–50% increase in both NPT and NS3 protein synthesis after a 4-hour nocodazole treatment. Since the translation of these two proteins was under the regulation of different sequence elements, these results suggest that the increase in HCV protein translation was not due to specific enhancement of HCV IRES-mediated translational activity. We also tested the effects of the nocodazole treatment on the NPT synthesis in the neomycin-resistant Huh-Neo cells, in which NPT is expressed from an integrated plasmid DNA. In contrast to HCV replicon cells, NPT synthesis in Huh-Neo cells was not affected by the nocodazole treatment (Fig. 2D,), indicating that the increase in HCV protein synthesis by the nocodazole treatment in HCV replicon cells was not due to enhancement of global translation.

These results are unexpected, raising a possibility that the newly-synthesized HCV RNA may be used for RNA translation in situ, without being transported away from the site of RNA synthesis. This result brought up an intriguing possibility that HCV RNA replication and translation are coupled and take place in the same replication complex.

HCV RNA Translation is Dependent on the Transcriptional Activity of the RNA

To test the idea that the newly synthesized HCV RNA is used for translation in situ, we then investigated whether translation was dependent on active RNA synthesis. We used a specific NS5B polymerase inhibitor, Benzothiadiazine [34,35], to inhibit HCV RNA synthesis and then examined the possible effects, if any, on HCV translation.

We first determined the efficiency and specificity of the inhibitor on ^{3}H-uridine incorporation (Fig. S1A). Huh7-N1b replicon cells were pretreated with or without Benzothiadiazine for 16 hours and then with actinomycin D for an additional 1 hour prior to ^{3}H-uridine labeling. Under this condition, ^{3}H-uridine is expected to be incorporated into HCV RNA only, but not cellular RNA [30]. The data showed that, in Huh7 cells, actinomycin D almost completely inhibited uridine incorporation. However, in Huh-N1b cells, actinomycin D did not completely inhibit ^{3}H-uridine incorporation; the residual incorporation likely represents HCV RNA synthesis, as confirmed by the autoradiography of the RNA products (Fig. S1A, lower panel). This residual RNA synthesis was inhibited by Benzothiadiazine. Furthermore, the Br-UTP label in Huh-N1b cells was detected as speckles in the perinuclear region; these speckles were not visible when the cells were treated with Benzothiadiazine (Fig. S1B). These results together indicate that Benzothiadiazine inhibits viral RNA synthesis specifically.

We also studied the effects of Benzothiadiazine on the steady-state level of replicon RNA by realtime RT-PCR analysis. The data showed that even after 16 hours of treatment, the total amount of replicon RNA in the cells was not significantly affected (Fig. S1C). Furthermore, the size of HCV RNA remained the same even after 16 hours of Benzothiadiazine treatment. After 2 days of treatment, however, the amounts of the replicon RNA decreased by about 50%. After 5 days, the RNA level dropped to 10% that of the control cells (Fig. S1D). As a comparison, nocodazole, which was reported to inhibit HCV RNA replication [33], had a smaller effect on the amounts of HCV RNA.

Having established the specificity of Benzothiadiazine on HCV RNA synthesis, we then labeled the Benzothiadiazine-treated cells with ^{35}S-Met and immunoprecipitated HCV proteins from the cell extracts (Fig. 3A). At 4 hour post-treatment, the amounts of newly synthesized HCV NS3 and NPT proteins were significantly decreased after the Benzothiadiazine treatment (Fig. 3A), while the amount and size of HCV RNA were not significantly affected, as determined by realtime RT-PCR and Northern blot (Fig. 3B). In contrast, in Huh-Neo cells, the Benzothiadiazine treatment did not affect the translation of NPT (Fig. 3A), indicating that Benzothiadiazine specifically inhibited translation of HCV RNA.

We further used a replication-defective replicon RNA (GND mutation in the NS5B region) to assess if active RNA replication of HCV is required for HCV protein translation. A separate experiment using an *in vitro* translation system showed that both wild-type HCV replicon and its GND mutant RNAs could produce equivalent amounts of NS2 to NS5B proteins (data not shown), indicating that the open reading frames in these RNAs are intact. The wild-type HCV replicon (Rep) and its GND mutant

HCV(JFH1)-infected Huh7.5 cells

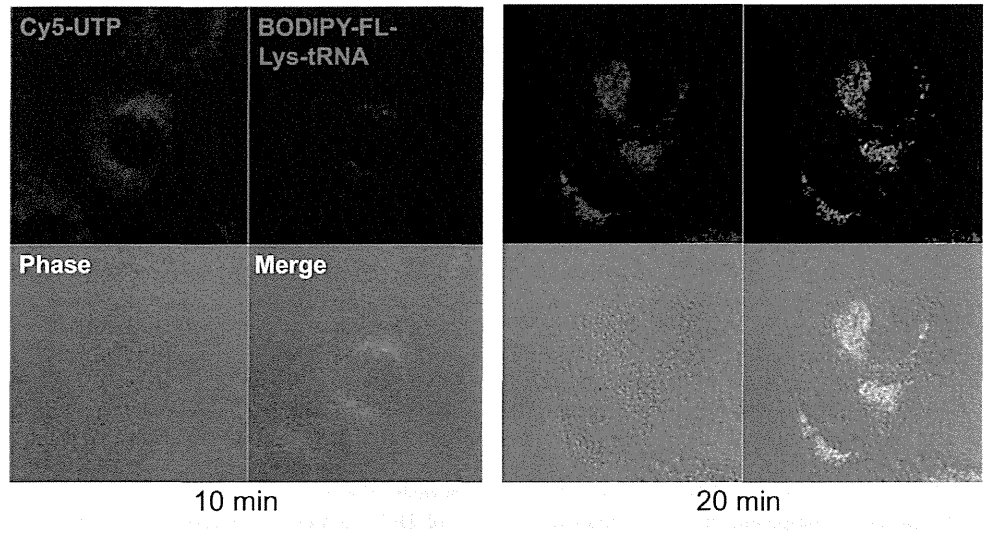

10 min

20 min

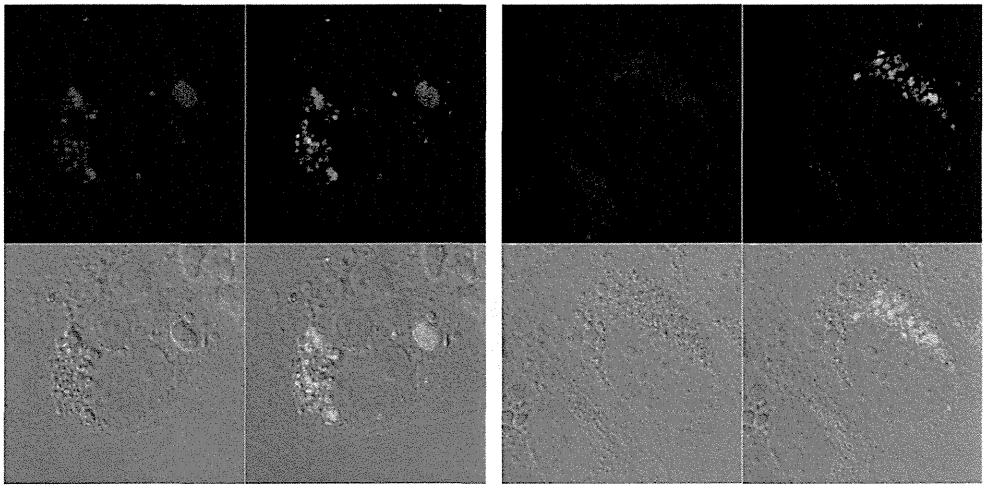

30 min

40 min

Huh7.5 cells

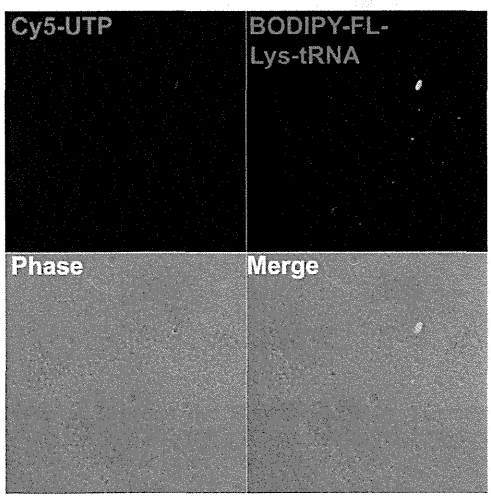

40 min

Figure 4. Double-labeling of newly-synthesized HCV RNA and newly synthesized viral peptides in JFH1-infected Huh-7.5 cells. Huh7.5 cells were infected with HCV JFH-1 strain for 2 days, and then were labeled with Cy5-UTP and BODIPY-FL-Lys-tRNA in the presence of actinomycin D and hippuristanol, which inhibit host RNA and protein synthesis, respectively. The cells were kept in 37°C chamber supplied with CO_2 for live cell imaging on a Zeiss LSM 510 laser scanning confocal microscope. Images were taken after 10–40 minutes of chase. Newly-synthesized HCV RNA was the first to be detected (as shown in red) and was in a perinuclear pattern. Newly-translated HCV viral peptides (as shown in green) were detected at later time points, completely co-localized with the sites of RNA synthesis. No significant amount of Cy5-UTP and BODIPY-FL-Lys-tRNA labeling could be detected in naïve Huh7.5 cells (as a negative control) in the presence of actinomycin D and hippuristanol.
doi:10.1371/journal.pone.0043600.g004

(Rep*GND) RNAs were then transfected into Huh7 cells, and the transfected cells were metabolically labeled with ^{35}S-Met for 14 hours to detect protein syntheses by immunoprecipitation with anti-NS3 or -NPT antibodies. The result showed that, the GND mutant yielded very little NS3 as compared with the corresponding wildtype replicon RNA (Fig. 3C). The amounts of wildtype and mutant RNAs were equivalent at 14 hours post RNA electroporation (Fig. 3D). This result suggested that HCV RNA replication enhanced the efficiency of HCV RNA translation, but could not rule out the possibilities that this enhanced translation was due to quicker degradation of the Rep*GND mutant and/or a higher copy number of the Rep RNA as a result of RNA replication. To further investigate if replication-competent HCV replicon RNA was preferentially translated, we compared the translation activity of a bicistronic Firefly luciferase replicon RNA (Luc-Rep) and the comparable but replication-defective Renilla luciferase replicon GND mutant (RLuc-RepGND) (Fig. 3E). Both constructs were first tested by *in vitro* translation assay to ensure that the both reporters were functional (data not shown). Immediately after transfection into Huh7 cells, both luciferase activities were equivalent initially; however, the FFLuc/RLuc ratio increased over time (Fig. 3F). The reverse paired replicons, RLuc-Rep and Luc-GND, also gave a similar result (Fig. 3G). We observed 2–4 folds more luciferase activities translated from the replication-competent replicon RNA than those from the GND mutants at 8 hr post-transfection (Fig. 3F & G), at which time the incoming RNAs had not yet been degraded, indicating that the replication-competent HCV RNA was preferentially translated.

We further performed a similar study using the infectious HCV clone JFH1 and its replication-defective mutant, JFH1-GND, in a time-course study of HCV protein translation. Huh7 cells were transfected with JFH1 or JFH1/GND RNA, labeled with ^{35}S-Met during the 0–8, 8–16, or 16–24 hours post-transfection, and followed by immunoprecipitation. The amounts of these two RNAs at 24 hours post-transfection were almost the same (Fig. S2B). However, only the infectious JFH RNA, but not its GND

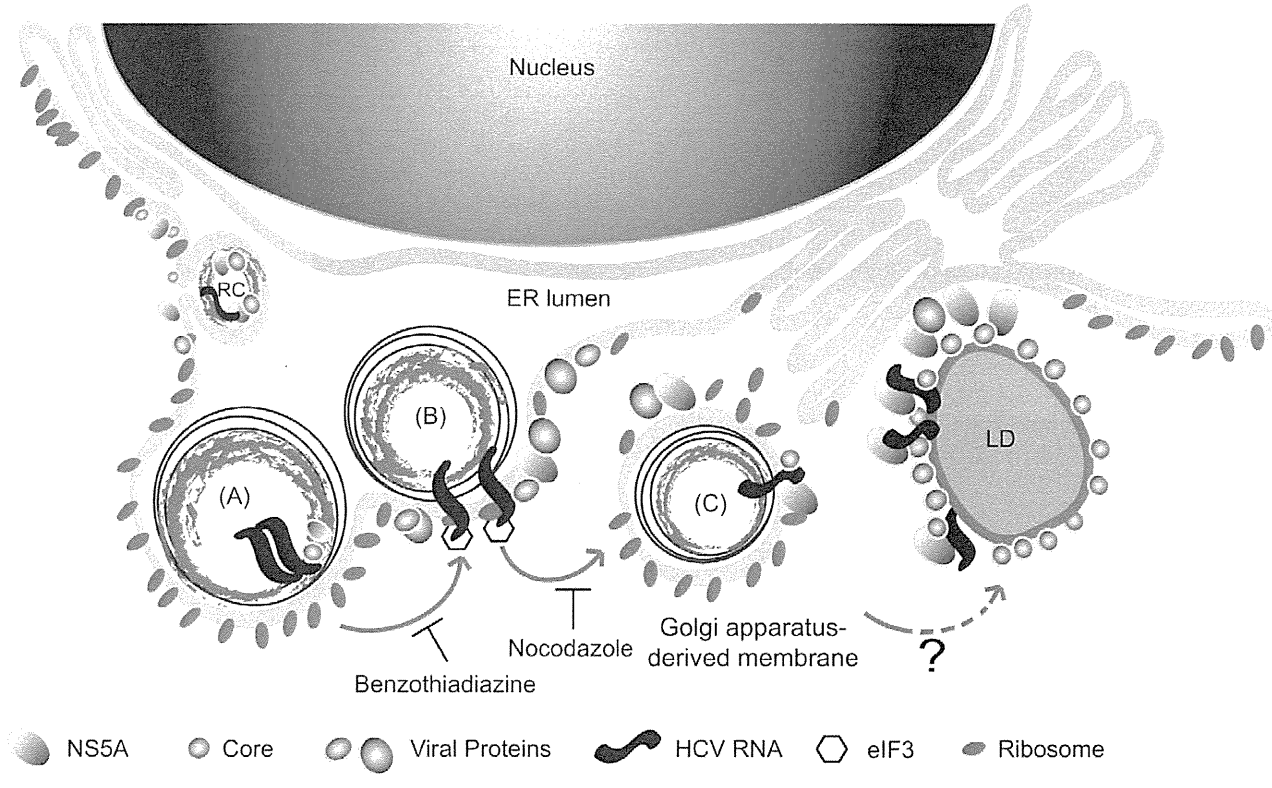

Figure 5. The proposed model of coupled replication/translation of HCV RNA. A proposed model of HCV replication-translation complex "replicasome". As reported, HCV replication complexes are assembled at ER, and then bud into the ER lumen. Consequently, (A) HCV RNA replication is first initiated in the multi-layered vesicle structure derived from the ER membrane. (B) The newly synthesized HCV RNA is translated around the ER-derived vesicle [39], where there are membrane-associated ribosomes. Benzothiadiazine blocks HCV RNA transcription and therefore decreases translation. (C) The newly-synthesized HCV RNA is later transported away from ER; nocodazole inhibits this transportation. HCV RNA is then transported to Golgi-derived membrane and/or then the lipid droplet (LD) for packaging and assembly of virus particles.
doi:10.1371/journal.pone.0043600.g005

mutant, yielded detectable amounts of NS3 and NS5A at 16–24 hours posttransfection (Fig. S2A). The kinetics of HCV protein synthesis corresponded well with the previously reported kinetics of HCV RNA synthesis following HCV (JFH1) RNA transfection [36]. The result further supported the conclusion that the replication of HCV RNA is required for competent HCV RNA translation.

We next assessed if the replication and translation of HCV RNA occurred in the same subcellular localizations. Huh7.5 cells were infected with HCV (JFH1); at 2 days after infection, the cells were labeled with Cy5-UTP and BODIPY-FL-lys-tRNA in the presence of hippuristanol and actinomycin D, which blocked eIF4A-dependent translation and host RNA transcription, respectively [27,37]. Under such a condition, Cy5-UTP will label newly synthesized HCV RNA, while BODIPY-FL-lys-tRNA will label only the newly synthesized HCV proteins since HCV translational initiation does not require eIF4A, which is blocked by hippuristanol [38]. A control experiment showed that neither dyes labeled the uninfected Huh7.5 cells (Fig. 4, lower panel). JHF-1-infected Huh7.5 cells were labeled with Cy5-UTP and BODIPY-FL-lys-tRNA for 15 minutes and then chased in unlabeled media from 10 to 40 minutes. The Cy5-U label could be detected at the early time point (10 min.) in the perinuclear region; BODIPY-FL-Lys-tRNA-labeled peptides were detected sparingly at this time, but gradually increased in intensity at later time points (Fig. 4). The earlier detection of Cy5-U label than BODIPY-FL-lys-tRNA label may have been due to the more efficient incorporation and more sensitive detection of the former label. Strong BODIPY-FL-lys-tRNA labeling signals were detected after 30 minutes of chase. Significantly, all of the BODIPY-FL-lys-tRNA labeled peptide colocalized with Cy5-U-labeled RNA at all the time points studied (Fig. 4). These findings suggest that HCV protein translation occurs on the newly synthesized RNA, and thus is likely coupled with RNA synthesis. From all the results above, we conclude that HCV RNA replication activity is a prerequisite to the efficient translation of HCV RNA.

Discussion

The mechanisms of replication and translation of HCV RNA have been extensively studied in the past few years. However, the exact subcellular localization of HCV RNA replication and translation is still unclear. Evidence has previously been presented that HCV RNA replication occurs on the detergent-resistant membrane (DRM) possibly derived from the ER [23,39]. In this report, the newly synthesized RNA was shown to be transported by the anterograde vesicle transport pathway. The microtubule-dependent mobility of newly-synthesized HCV RNA or the replication complex has also been described elsewhere [40]. Our data in this study further showed that the nocodazole treatment inhibited the transportation of the newly-synthesized RNA from the ER-derived replication complex to Golgi but did not inhibit the initiation of HCV RNA replication, since BrUTP labeling of HCV RNA occurred normally in the presence of nocodazole (Fig. 2). Intuitively, the newly-synthesized HCV RNA is expected to be transported to the site of the cellular translation machinery, similar to the case for cellular mRNAs, which are synthesized in the nucleus and transported to the cytoplasmic translation machinery for protein synthesis. However, we instead found that the movement of the HCV RNA from the ER to Golgi was not required for HCV translation, suggesting that the newly synthesized HCV RNA is used for translation near the site of HCV RNA synthesis before being transported away. Furthermore, we showed that active RNA replication was a prerequisite for efficient HCV translation. This conclusion was demonstrated using four different approaches, including studying the effects of an HCV RNA polymerase inhibitor on HCV protein translation (Fig. 3A), comparing the translation efficiencies of wildtype and replication-defective replicons (Fig. 3C) and those of infectious and non replicating JFH strain of HCV (Fig. S2A), and also by determining the relative translation efficiencies of the replicating and non-replicating dual luciferase reporter plasmids (Figs. 3F–G). Finally, we showed that the newly synthesized viral proteins almost completely colocalized with the newly synthesized viral RNA, suggesting that the sites of HCV RNA replication and protein translation nearly overlap. This mechanism of coupled RNA replication and translation may explain the previous findings that many cellular proteins, such as PTB [9,26], La antigen [10,13] and SYNCRIP [11,14], are involved in both the replication and translation in the HCV life cycle. The close proximity of these two machineries will allow for ready switches between translation and replication.

Although coupling of translation and RNA replication has been reported for many RNA viruses [16,17,41,42]_ENREF_37, the HCV case appears to be unique. For example, translation and replication of poliovirus RNA are coupled, but in the sense that RNA transcription is dependent on viral translation in *cis* [16]. Insertion of an early termination codon resulted in lower efficiency of poliovirus RNA replication. The translation and replication are regulated by the binding of different cellular or viral proteins to the 5? UTR of poliovirus RNA [43–45]. Also, the microtubule-dependent movement of poliovirus viral RNA is associated with the replication activity of viral RNA [46]. While the inactive replication complexes reside at microtubule-organizing center (MTOC), the replicating viral RNA is localized at the perinuclear sites [46]. Thus, the RNA movement is required for poliovirus replication, in contrast to the situation with HCV. In HCV, nocodazole did not inhibit viral RNA replication; also, the newly-synthesized HCV RNA failed to exit from ER after the nocodazole treatment and yet, protein translation increased; thus, the cytoskeleton-assisted movement of the newly-synthesized HCV RNA is not required for RNA translation. Thus, in HCV, the observed movement of the viral RNA from the ER-derived to the Golgi-derived membrane appears to be required for other steps of HCV replication, rather than protein translation. Due to the fact that the viral structural proteins are absent in the HCV replicon cells, this RNA movement is likely mediated by viral NS proteins, such as NS5A, which has been reported to target Golgi apparatus [47]. In a kinetics study examining the appearance of the newly synthesized HCV RNA and HCV proteins in the HCV (JFH-1)-infected cell, we also found that all of the newly synthesized proteins were at the site of newly synthesized RNA (Fig. 4). Thus, there appears to be a replication complex that carries out both replication and translation. This concept is novel to the known mechanisms of RNA virus translation and transcription.

These findings raised an important issue, namely, how the initial viral translation is carried out, since, as a positive-strand RNA virus, the very initial round of translation from the incoming HCV viral genome has to take place before viral RNA replication can occur. Conceivably, the free viral RNA genome generated by uncoating of the incoming virion in the endosome (or from the transfected viral RNA or replicons) can associate with ribosomes on the rough ER and be translated in an RNA replication-independent manner. Such translation is likely of low efficiency, but is sufficient to support first round of HCV RNA translation. These initial viral protein products and RNAs will then be encased into the membranous replication complex and become part of the

replication-translation machinery. The latter process will then become the main mechanism of HCV replication-translation.

In summary, we propose the following pathway for HCV RNA replication and translation (Fig. 5). Previous studies have shown that HCV RNA replication takes place in an ER-derived membranous vesicle [39]. The newly-synthesized viral RNA will be translated immediately after being synthesized in or around the vesicle. Benzothiadiazine treatments inhibited HCV RNA transcription and therefore inhibited HCV RNA translation as well (Fig. 5, A–B). After translation has occurred, HCV RNA is then transported via anterograde vesicle trafficking pathway away from the ER to a membrane compartment associated with the Golgi apparatus (Fig. 5C). Several other reports suggest that HCV RNA may be transported along with viral proteins (core and NS5A) to lipid droplets, where viral assembly takes place [48]; however, the kinetics of this process is unclear. Further studies in dissecting HCV RNA transportation during HCV infection will be valuable for understanding HCV life cycle comprehensively. In conclusion, this replication and translation machinery constitutes the viral "replicasome", which may reflect the membranous webs observed previously.

Supporting Information

Figure S1 Benzothiadiazine treatment in Huh-N1b replicon cells. Huh7 and Huh-N1b cells pre-treated with actinomycin D, Benzothiadiazine (NS5B inhibitor), or combination of both for 4 hours, and then labeled with ^{3}H-Uridine (A) or BrUTP (B). RNA synthesis was detected by RNA precipitation followed by scintillation counting (A), by immunofluorescence staining (B), or by real-time RT-PCR (C, D). Autoradiography of the H^{3}-uridine-labeled RNA was also performed (bottom, panel A). The relative amounts of intracellular HCV RNA after the various treatments are shown in (C, D). Benzothiadiazine specifically inhibited viral transcription, but did not affect the intracellular replicon RNA levels under this condition (C). (D), long-term Benzothiadiazine treatment (over 2 days) significantly decreased the replicon RNA levels.
(TIF)

Figure S2 Preferential translation of JFH1 wildtype over the GND mutant HCV RNA. (A) A time-course study of HCV NS protein translation in cells transfected with JFH1 or its GND mutant. The cells were labeled with S^{35}-methionine from 0–8, 8–16 and 16–24 hours posttransfection and followed by immunoprecipitation with anti-NS3 or HCV patient serum. NS3 and NS5A were detected by immunoprecipitation and separated by SDS-PAGE. (B) The corresponding intracellular HCV RNA levels in (A). The intracellular RNA levels at 24 hour post-transfection were determined by real-time RT-PCR.
(TIF)

Acknowledgments

Special thanks are to Specialized Microscopy Core of Doheny Eye Institute at USC, and Microscope Subcore of the USC Center for Liver Disease.

Author Contributions

Conceived and designed the experiments: HML ML. Performed the experiments: HML HA. Analyzed the data: HML JO ML. Contributed reagents/materials/analysis tools: HML HA KM. Wrote the paper: HML ML.

References

1. Reed KE, Rice CM (2000) Overview of hepatitis C virus genome structure, polyprotein processing, and protein properties. Curr Top Microbiol Immunol 242: 55–84.
2. Lohmann V, Korner F, Koch J, Herian U, Theilmann L, et al. (1999) Replication of subgenomic hepatitis C virus RNAs in a hepatoma cell line. Science 285: 110–113.
3. Penin F, Brass V, Appel N, Ramboarina S, Montserret R, et al. (2004) Structure and function of the membrane anchor domain of hepatitis C virus nonstructural protein 5A. J Biol Chem 279: 40835–40843.
4. Gosert R, Egger D, Lohmann V, Bartenschlager R, Blum HE, et al. (2003) Identification of the hepatitis C virus RNA replication complex in Huh-7 cells harboring subgenomic replicons. J Virol 77: 5487–5492.
5. Lee KJ, Choi J, Ou JH, Lai MM (2004) The C-terminal transmembrane domain of hepatitis C virus (HCV) RNA polymerase is essential for HCV replication in vivo. J Virol 78: 3797–3802.
6. Gao L, Aizaki H, He JW, Lai MM (2004) Interactions between viral nonstructural proteins and host protein hVAP-33 mediate the formation of hepatitis C virus RNA replication complex on lipid raft. J Virol 78: 3480–3488.
7. Goueslain L, Alsaleh K, Horellou P, Roingeard P, Descamps V, et al. (2009) Identification of Gbf1 as a Cellular Factor Required for Hepatitis C Virus Rna Replication. J Virol.
8. Manna D, Aligo J, Xu C, Park WS, Koc H, et al. (2009) Endocytic Rab proteins are required for hepatitis C virus replication complex formation. Virology.
9. Chang KS, Luo G (2006) The polypyrimidine tract-binding protein (PTB) is required for efficient replication of hepatitis C virus (HCV) RNA. Virus Res 115: 1–8.
10. Domitrovich AM, Diebel KW, Ali N, Sarker S, Siddiqui A (2005) Role of La autoantigen and polypyrimidine tract-binding protein in HCV replication. Virology 335: 72–86.
11. Liu HM, Aizaki H, Choi KS, Machida K, Ou JJ, et al. (2009) SYNCRIP (synaptotagmin-binding, cytoplasmic RNA-interacting protein) is a host factor involved in hepatitis C virus RNA replication. Virology 386: 249–256.
12. Kapadia SB, Chisari FV (2005) Hepatitis C virus RNA replication is regulated by host geranylgeranylation and fatty acids. Proc Natl Acad Sci U S A 102: 2561–2566.
13. Ali N, Pruijn GJ, Kenan DJ, Keene JD, Siddiqui A (2000) Human La antigen is required for the hepatitis C virus internal ribosome entry site-mediated translation. J Biol Chem 275: 27531–27540.
14. Kim JH, Paek KY, Ha SH, Cho S, Choi K, et al. (2004) A cellular RNA-binding protein enhances internal ribosomal entry site-dependent translation through an interaction downstream of the hepatitis C virus polyprotein initiation codon. Mol Cell Biol 24: 7878–7890.
15. Ito T, Lai MM (1999) An internal polypyrimidine-tract-binding protein-binding site in the hepatitis C virus RNA attenuates translation, which is relieved by the 3'-untranslated sequence. Virology 254: 288–296.
16. Novak JE, Kirkegaard K (1994) Coupling between genome translation and replication in an RNA virus. Genes Dev 8: 1726–1737.
17. Sanz MA, Castello A, Carrasco L (2007) Viral translation is coupled to transcription in Sindbis virus-infected cells. J Virol 81: 7061–7068.
18. Iost I, Dreyfus M (1994) mRNAs can be stabilized by DEAD-box proteins. Nature 372: 193–196.
19. Iost I, Dreyfus M (1995) The stability of Escherichia coli lacZ mRNA depends upon the simultaneity of its synthesis and translation. Embo J 14: 3252–3261.
20. Nakabayashi H, Taketa K, Miyano K, Yamane T, Sato J (1982) Growth of human hepatoma cells lines with differentiated functions in chemically defined medium. Cancer Res 42: 3858–3863.
21. Blight KJ, McKeating JA, Rice CM (2002) Highly permissive cell lines for subgenomic and genomic hepatitis C virus RNA replication. J Virol 76: 13001–13014.
22. Guo JT, Bichko VV, Seeger C (2001) Effect of alpha interferon on the hepatitis C virus replicon. J Virol 75: 8516–8523.
23. Aizaki H, Lee KJ, Sung VM, Ishiko H, Lai MM (2004) Characterization of the hepatitis C virus RNA replication complex associated with lipid rafts. Virology 324: 450–461.
24. Shi ST, Lee KJ, Aizaki H, Hwang SB, Lai MM (2003) Hepatitis C virus RNA replication occurs on a detergent-resistant membrane that cofractionates with caveolin-2. J Virol 77: 4160–4168.
25. Wakita T, Pietschmann T, Kato T, Date T, Miyamoto M, et al. (2005) Production of infectious hepatitis C virus in tissue culture from a cloned viral genome. Nat Med 11: 791–796.
26. Aizaki H, Choi KS, Liu M, Li YJ, Lai MM (2006) Polypyrimidine-tract-binding protein is a component of the HCV RNA replication complex and necessary for RNA synthesis. J Biomed Sci 13: 469–480.
27. Bordeleau ME, Mori A, Oberer M, Lindqvist L, Chard LS, et al. (2006) Functional characterization of IRESes by an inhibitor of the RNA helicase eIF4A. Nat Chem Biol 2: 213–220.
28. Iborra FJ, Jackson DA, Cook PR (2001) Coupled transcription and translation within nuclei of mammalian cells. Science 293: 1139–1142.

29. Hamamoto I, Nishimura Y, Okamoto T, Aizaki H, Liu M, et al. (2005) Human VAP-B is involved in hepatitis C virus replication through interaction with NS5A and NS5B. J Virol 79: 13473–13482.
30. Choi J, Lee KJ, Zheng Y, Yamaga AK, Lai MM, et al. (2004) Reactive oxygen species suppress hepatitis C virus RNA replication in human hepatoma cells. Hepatology 39: 81–89.
31. Watson P, Forster R, Palmer KJ, Pepperkok R, Stephens DJ (2005) Coupling of ER exit to microtubules through direct interaction of COPII with dynactin. Nat Cell Biol 7: 48–55.
32. Lippincott-Schwartz J, Cole NB, Marotta A, Conrad PA, Bloom GS (1995) Kinesin is the motor for microtubule-mediated Golgi-to-ER membrane traffic. J Cell Biol 128: 293–306.
33. Bost AG, Venable D, Liu L, Heinz BA (2003) Cytoskeletal requirements for hepatitis C virus (HCV) RNA synthesis in the HCV replicon cell culture system. J Virol 77: 4401–4408.
34. Hirashima S, Suzuki T, Ishida T, Noji S, Yata S, et al. (2006) Benzimidazole derivatives bearing substituted biphenyls as hepatitis C virus NS5B RNA-dependent RNA polymerase inhibitors: structure-activity relationship studies and identification of a potent and highly selective inhibitor JTK-109. J Med Chem 49: 4721–4736.
35. Tedesco R, Shaw AN, Bambal R, Chai D, Concha NO, et al. (2006) 3-(1,1-dioxo-2H-(1,2,4)-benzothiadiazin-3-yl)-4-hydroxy-2(1H)-quinolinones, potent inhibitors of hepatitis C virus RNA-dependent RNA polymerase. J Med Chem 49: 971–983.
36. Bartenschlager R (2006) Hepatitis C virus molecular clones: from cDNA to infectious virus particles in cell culture. Curr Opin Microbiol 9: 416–422.
37. Goldberg IH, Rabinowitz M, Reich E (1962) Basis of actinomycin action. I. DNA binding and inhibition of RNA-polymerase synthetic reactions by actinomycin. Proc Natl Acad Sci U S A 48: 2094–2101.
38. Kieft JS, Zhou K, Grech A, Jubin R, Doudna JA (2002) Crystal structure of an RNA tertiary domain essential to HCV IRES-mediated translation initiation. Nat Struct Biol 9: 370–374.
39. Sir D, Kuo CF, Tian Y, Liu HM, Huang EJ, et al. (2012) Replication of Hepatitis C Virus RNA on Autophagosomal Membranes. The Journal of Biological Chemistry in press.
40. Wolk B, Buchele B, Moradpour D, Rice CM (2008) A dynamic view of hepatitis C virus replication complexes. J Virol 82: 10519–10531.
41. Annamalai P, Rao AL (2006) Packaging of brome mosaic virus subgenomic RNA is functionally coupled to replication-dependent transcription and translation of coat protein. J Virol 80: 10096–10108.
42. Egger D, Teterina N, Ehrenfeld E, Bienz K (2000) Formation of the poliovirus replication complex requires coupled viral translation, vesicle production, and viral RNA synthesis. J Virol 74: 6570–6580.
43. Toyoda H, Franco D, Fujita K, Paul AV, Wimmer E (2007) Replication of poliovirus requires binding of the poly(rC) binding protein to the cloverleaf as well as to the adjacent C-rich spacer sequence between the cloverleaf and the internal ribosomal entry site. J Virol 81: 10017–10028.
44. Perera R, Daijogo S, Walter BL, Nguyen JH, Semler BL (2007) Cellular protein modification by poliovirus: the two faces of poly(rC)-binding protein. J Virol 81: 8919–8932.
45. Gamarnik AV, Andino R (2000) Interactions of viral protein 3CD and poly(rC) binding protein with the 5' untranslated region of the poliovirus genome. J Virol 74: 2219–2226.
46. Egger D, Bienz K (2005) Intracellular location and translocation of silent and active poliovirus replication complexes. J Gen Virol 86: 707–718.
47. Shi ST, Polyak SJ, Tu H, Taylor DR, Gretch DR, et al. (2002) Hepatitis C virus NS5A colocalizes with the core protein on lipid droplets and interacts with apolipoproteins. Virology 292: 198–210.
48. Miyanari Y, Atsuzawa K, Usuda N, Watashi K, Hishiki T, et al. (2007) The lipid droplet is an important organelle for hepatitis C virus production. Nat Cell Biol 9: 1089–1097.